Past and future of the Arctic sea ice in HighResMIP climate models

Julia Selivanova[1,2], Doroteaciro Iovino[1], Francesco Cocetta[1]

[1] CMCC Foundation - Euro-Mediterranean Center on Climate Change, Italy

[2] University of Bologna, Department of Physics and Astronomy, Bologna, Italy

Correspondence to: Julia Selivanova (julia.selivanova@cmcc.it)

Abstract.

We examine the past and projected changes in Arctic sea ice properties in 6 climate models participating in the High Resolution Model Intercomparison Project (HighResMIP) in the Coupled Model Intercomparison Project Phase 6 (CMIP6). Within HighResMIP each of the experiments are run using a reference resolution configuration (consistent with typical CMIP6 runs) and higher resolution configurations. The role of horizontal grid resolution in both the atmosphere and ocean model components in reproducing past and future changes in the Arctic sea ice cover is analysed. Model outputs from the coupled historical (hist-1950) and future (highres-future) runs are used to describe the multi-model, multi-resolution representation of the Arctic sea ice and to evaluate the systematic differences (if any) that resolution enhancement causes. Our results indicate that there is not a strong relationship between the representation of sea ice cover and the ocean/atmosphere grids; the impact of horizontal resolution depends rather on the examined sea ice characteristic and the model used. However, the refinement of the ocean grid has a more prominent effect compared to the atmospheric one, with eddy-permitting ocean configurations providing generally more realistic representations of sea ice area and sea ice edge. All models project substantial sea ice shrinking: the Arctic loses nearly 95% of sea ice volume from 1950 to 2050. The model selection based on historical performance potentially improves the accuracy of the model projections and predicts the Arctic to turn ice-free as early as in 2047. Along with the overall sea ice loss, changes in the spatial structure of the total sea ice and its partition in ice classes are noticed: the marginal ice zone (MIZ) will dominate the ice cover by 2050 suggesting a shift to a new sea ice regime much closer to the current Antarctic sea ice conditions. The MIZ-dominated Arctic might drive developments and modifications of model physics and parameterizations in the new generation of GCMs.

1 Introduction

Sea ice is the key feature of high-latitude climate through its role in the surface energy budget, ocean and atmosphere dynamics, and marine ecosystems. Over the recent decades, the Arctic has witnessed unprecedented sea ice loss,

30 which is a key indicator of global climate change (e.g. Onarheim et al., 2018; Serreze and Meier, 2019), driven both by
31 anthropogenic activities and internal climate variability (e.g. Notz and Stroeve, 2016). Arctic sea ice has declined in every
32 month of the year with the strongest trends in September, a sea ice extent (SIE) reduction of 79000 km^2 yr^{-1} in the period
33 1979-2022, compared to that in March, with -39200 km^2 yr^{-1} over 1979-2022 (http://nsidc.org/arcticseaicenews/2022/). The
34 overall decrease in SIE reveals large seasonal and regional variability. Although winter sea ice loss is dominated by the
35 reduction in the Barents Sea (Årthun et al., 2021), the most pronounced summer sea ice decrease occurs in the East Siberian
36 Sea (that explains more than 20% of the September trend, (Watts et al., 2021) and in the Beaufort, Chukchi, Laptev and Kara
37 seas (Onarheim et al., 2018). Along with a severe reduction in sea ice coverage, Arctic sea ice has also thinned, with a ~70%
38 reduction in summer sea ice volume (SIV) from 1979 to 2021 (https://nsidc.org/). As a consequence, the Arctic ice is getting
39 younger: the portion of the multi-year ice, which previously was the iconic feature of the Arctic, has decreased from ~30% in
40 1985 (beginning of the satellite era) to ~4.4% in 2020 in winter months (Perovich et al., 2020). The Arctic transition toward
41 a first-year ice regime might substantially alter the interactions in the ocean-atmosphere-ice system (Aksenov et al., 2017).
42 The changes in total SIE and sea ice thickness (SIT) cause a redistribution of the sea ice classes, in particular the marginal
43 ice zone (MIZ) is strongly affected (Rolph et al., 2020). The Arctic MIZ has held interest as the fundamental region
44 supporting many physical, biological and biogeochemical processes (Tàpias et al., 2021). The MIZ is traditionally defined as
45 the region where polar air, ice, and water masses interact with the ocean temperature and subpolar climate system (Wadhams
46 and Deacon, 1981). It corresponds to the portion of the ice-covered ocean often characterised by highly variable ice
47 conditions, where surface gravity waves significantly impact the dynamics of sea ice (e.g. Dumont et al., 2011). Due to the
48 large uncertainties in observed and forecasted waves within sea ice, the MIZ is still operationally defined through a sea ice
49 concentration (SIC) thresholds, as the transition zone between open water and consolidated pack ice, where the total area of
50 the ocean is covered by 15-80% of sea ice (e.g. Strong, 2017; Paul et al., 2021; Rolph et al., 2020). While there are no
51 significant changes in the area of the Arctic MIZ during the satellite era (Rolph et al., 2020), the marginal ice zone fraction
52 (MIZF) defined as the percentage of total sea ice area (SIA) covered by MIZ (Horvat, 2021) increases by more than 50% in
53 August and September as the total SIA drastically decreases (Rolph et al., 2020; Horvat, 2021). Since the MIZ differs from
54 the pack ice in higher sensitivity to the dynamic and thermodynamic forces, the growing MIZF changes the Arctic response
55 to global warming, which may worsen the pace of sea ice melt and pose repercussions for local and global climate.

56   Assuming that the Arctic Ocean will continue to lose sea ice, a relevant question is how fast the Arctic will turn
57 ice-free in summer. Coupled climate models can be used in the prediction and projection of the climate system, including the
58 sea ice conditions. In the majority of simulations from CMIP6 (Eyring et al., 2016), the Arctic Ocean becomes practically
59 sea ice free (SIA < 1 million km^2) in September for the first time before 2050 in all scenarios (Notz and SIMIP Community,
60 2020) or even by 2035 when selecting only the models that best represent the present Arctic sea ice state and northward
61 ocean heat transport (Docquier and Koenigk, 2021). Even using a process-based selection criterion, uncertainties in the
62 model projections are relatively large, which undermines the model's trustworthiness (Docquier and Koenigk, 2021).
63 Besides, the accurate simulation of past and present Arctic sea ice is still challenging. Although the CMIP6 multi-model

ensemble mean is closer to the observed sensitivity of Arctic sea ice to global warming (Notz and SIMIP Community, 2020; Shu et al., 2020), there is little difference in overall model performance among CMIP3, CMIP5 and CMIP6. CMIP6 models still simulate a wide spread of mean sea ice area and volume in March and September (Davy and Outten, 2020; Notz and SIMIP Community, 2020; Watts et al., 2021).

Among the model developments and improvements needed to produce more accurate future projections, the increase in horizontal spatial resolution is recognized to be a key step to enhance the representation of the complex processes at high latitudes and to obtain trustworthy projections of ice variability. In order to address the impact of the model grid resolution on the simulated oceanic and atmospheric phenomena, the High-Resolution Model Intercomparison Project (HighResMIP; Haarsma et al., 2016) was designed within the EU Horizon 2020 PRIMAVERA project (PRocess-based climate sIMulation: AdVances in high-resolution modelling and European climate Risk Assessment, https://www.primavera-h2020.eu/). HighResMIP is one of the CMIP6-endorsed model intercomparison projects, which provides a useful framework to investigate the role of the enhanced horizontal resolution in representing the features of the climate system. A number of climate modelling groups contributed to the project providing the same simulations in at least two different configurations. The impact of the increased resolution within the HighResMIP is examined in many studies with regard to atmosphere, sea ice, and ocean components of the climate systems (e.g., Fuentes-Franco and Koenigk, 2019; Docquier et al., 2019; Bador et al., 2020; Roberts et al., 2020; Jackson et al., 2020; Lohmann et al., 2021; Meccia et al., 2021). Even though high-resolution models can resolve specific dynamical features, the role of the enhanced horizontal resolution is not uniform across ocean regions and models. Grist et al. (2018) demonstrated that refining the ocean grid to eddy-permitting resolution raises the Atlantic meridional heat transport and improves the agreement with observational estimates - they also show the significantly smaller impact of atmosphere resolution on the strength of the heat transport. Docquier et al. (2019) confirmed this finding and showed that a better representation of Atlantic surface characteristics, velocity fields, and sea surface temperature (in addition to transports toward the Arctic) improves the representation of the Arctic SIA and SIV. Nevertheless, the role of ocean resolution in the representation of ocean heat transport (OHT) and SIA is less clear when considering the regional effect on specific Arctic sectors, as shown for the Barents Sea in Docquier et al. (2020).

Here, we focus on the impact of horizontal resolution on the Arctic sea ice properties in the past and future at hemispheric and regional scales using the model outputs from coupled historical (hist-1950) and future (highres-future) runs from HighResMIP. We assess seasonal and interannual variability and trends in the SIA and SIV, and examine when the Arctic will see its first ice-free summer. We aim to explore the role of enhanced ocean/atmosphere horizontal resolution in the representation of past and current sea ice and to provide some insight into whether the grid refinement improves the model performance in predicting the future Arctic sea ice conditions.

2 Data

In this study, we analyse the outputs from the six coupled climate models participating in the HighResMIP. We use coupled runs with historical forcing (hist-1950) covering the period 1950-2014 and future projections (highres-future) from 2015 to 2050 based on the Fossil-fueled development SSP5-8.5 scenario. For the ocean, five models use the Nucleus for European Modelling of the Ocean framework (NEMO, Madec et al., 2016), yet different versions, whereas MPI-ESM is based on the Max Planck Institute Ocean Model (MPIOM, Jungclaus et al., 2013). The basic characteristics of the models are given in Table 1. Because each model uses at least two different resolutions, we evaluate 14 configurations in total. CMCC-CM2 and MPI-ESM use one ocean (eddy-permitting) resolution with two different atmospheric grids. ECMWF-IFS and EC-Earth3P run two of three configurations with an eddy-permitting ocean and different atmosphere resolutions. In other models, ocean and atmosphere resolutions vary in concert among configurations. ECMWF-IFS is not considered in the analysis of future projections since it does not provide the outputs from highres-future experiments. It is important to note that ECMWF-IFS, EC-Earth3P and CNRM benefit from several ensemble members (eight, three and six members for ECMWF LR, MR and HR, respectively; three members for both configurations of EC-Earth3P and CNRM). Given a small ensemble size of multi-ensemble configurations, a clear assessment of internal variability is not feasible in the context of this paper. We use only the first ensemble member in this study.

Table 1. Models and specifications of their configurations used in the study.

Model configuration		nominal ocean resolution (°)	nominal atmosphere resolution (km)	model components	
				ocean-sea ice	atmosphere
CMCC-CM2 (Cherchi et al., 2019)	HR	0.25	100	NEMO3.6+CICE4.0	CAM4
	VHR	0.25	25		
CNRM-CM6-1 (Voldoire et al., 2019)	LR	1	250	NEMO3.6+GELATO6	ARPEGE6.3
	HR	0.25	100		
ECMWF-IFS (Roberts et al., 2018)	LR	1	50	NEMO3.4+LIM2	IFS cycle43r1
	MR	0.25	50		
	HR	0.25	25		
EC-Earth3P (Haarsma et al., 2020)	LR	1	100	NEMO3.6+LIM3	IFS cycle36r1
	HR	0.25	50		

HadGEM3 (Williams et al., 2018)	LM	1	250	NEMO3.6+CICE5.1	UM
	MM	0.25	100		
	HM	0.25	50		
MPI-ESM (Müller et al., 2018)	HR	0.4	100	MPIOM1.6.3	ECHAM6.3
	XR	0.4	50		

112

113

114   For the past sea ice properties, we mainly focus on the time period from 1979 to compare model results with
115 available satellite records. The simulated SIA is validated against satellite observations. We use monthly SIC from two
116 satellite-based products: the NOAA/NSIDC Climate Data Record (version 4, Meier and Stewart., 2021, hereafter CDR) and
117 EUMETSAT OSISAF Climate Data Record and Interim Climate Data Record (release 2, products OSI-450 and OSI-430-b,
118 Lavergne et al., 2019) both for the period 1979-2021. CDR uses gridded brightness temperatures in low frequencies from the
119 Nimbus-7 SMMR (18, 37 GHz) and the DMSP series of SSM/I and SSMIS passive microwave radiometers (19.4, 22.2, 37
120 GHz). Different ratios of frequencies are used to filter weather effects. The output data are distributed on a 25 km x 25 km
121 polar stereographic grid. CDR algorithm blends the NASA Team (NT; Cavalieri et al., 1984) and the Bootstrap (BT; Comiso,
122 1986) by selecting the higher concentration value for each grid cell, so taking advantage of the strengths of each algorithm to
123 produce concentration fields that are more accurate than those from either algorithm alone (Meier, 2014). OSISAF comprises
124 two SIC products based on passive microwave sensors: OSI-450 (from 1979 to 2015) and OSI-430-b, extension from 2016
125 onwards. OSI-450 uses data from the SMMR 1979-1987), SSM/I (1987-2008), SSMIS (2006-2015) instruments (19.35 and
126 37 GHz frequencies) together with Era Interim reanalysis (Dee et al., 2011), while OSI-430-b is based on SSMIS and
127 operational analysis and forecast from ECMWF. We use estimates of SIT and SIV from the Pan-Arctic Ice Ocean Modeling
128 and Assimilation System (PIOMAS; Zhang and Rothrock, 2003) that comprises the global Parallel Ocean and sea Ice Model
129 (POIM) coupled to eight-category thickness and enthalpy distribution sea ice model and a data assimilation of SST (from
130 NCEP/NCAR reanalysis, Kalnay et al., 1996) and SIC (from the NSIDC near-real time product; Brodzik and Stewart, 2016).
131 PIOMAS proved its credibility against in-situ measurements (Stroeve et al., 2014; Wang et al., 2016) and therefore it is
132 widely used in numerous intercomparison studies as the observational proxy (e.g. Labe et al., 2018). Note that PIOMAS
133 tends to underestimate the thick ice north to Greenland and the Canadian Arctic Archipelago and overestimate SIT in the
134 areas of thin ice (Stroeve et al., 2014; Wang et al., 2016). Monthly fields of SIC and effective SIT from 1979 to 2021 are
135 used in this work. We describe sea ice coverage in terms of SIA (the integral sum of the product of ocean grid-cell areas and
136 the corresponding sea ice concentration), instead of SIE (the integral sum of the areas of all grid cells with at least 15% of
137 SIC). To compute SIV, the equivalent SIT (the sea ice volume per grid-cell area) is multiplied by the individual grid-cell

138 area, and then summed over the Arctic region. To derive integrative metrics, only the grid cells with at least 15% SIC are
139 considered owing to the high uncertainty in passive microwave retrievals in low sea ice conditions. Apart from model
140 evaluation at the hemispheric scale, we provide a regional analysis of sea ice variability in six subregions of the Arctic Ocean
141 (north of 65°N) as defined in Figure 1.

142 3 Results

143 3.1 Mean state

144   First, we assess the spatial patterns of simulated ice properties against observational-based estimates over the
145 historical period restricted from 1979 to 2014. Figure 2 shows the climatological mean distribution of SIT in March and
146 September for model outputs and PIOMAS. The mean position of 15% and 80% SIC edges is also shown from each model
147 and CDR (over PIOMAS). In general, most models struggle to reasonably simulate the spatial pattern of SIT and produce
148 either thicker (ECMWF-IFS, EC-Earth3P, CMCC-CM2 VHR4) or thinner (CNRM-CM6, MPI-ESM) ice over a vast area
149 compared to PIOMAS. Some models are able to correctly locate the thickest ice north of Greenland and the Canadian Arctic
150 Archipelago and the thinner ice in the Siberian Shelf Seas (HadGEM3, CMCC-CM2 HR4), but the simulated ice can thicken
151 up to 7 m. EC-Earth3P HR and ECMWF-IFS MR, despite capturing the overall SIT pattern, simulate high thickness also in
152 the East Siberian and Chukchi Seas, which is clearly visible in March. This might be related to unrealistic sea ice drift. As in
153 PIOMAS, most models reproduce changes in the SIT between March and September with a more pronounced seasonal
154 retreat in the Siberian sector.

155   There is no direct effect of horizontal resolution on the spatial distribution of SIT. Increasing ocean resolution, the
156 mean SIT decreases for ECMWF-IFS, does not change notably for HadGEM3 and CNRM-CM6, and increases for
157 EC-Earth3P. The role of atmosphere resolution also depends on the model: for example, the finer atmosphere resolution
158 MPI-ESM reproduces on average slightly thinner ice compared to LR configuration, while the finer CMCC-CM2 simulates
159 thicker ice over a larger area. Biases in the representation of SIT pattern can be related to poor representation in surface
160 pressure and large-scale atmospheric patterns (Kwok and Untersteiner, 2011; Stroeve et al., 2014), sea ice motion and ocean
161 forcing (Watts et al., 2021).

162   Most models tend to realistically simulate the position of the sea ice edge both in March and September. The LR
163 configuration of ECMWF-IFS tends to overestimate the sea ice cover far south in the North Atlantic and the North Pacific
164 Oceans compared to CDR. The bias can be explained by the poor representation of the ocean advection. Docquir et al.
165 (2019) showed that the northward OHT is improved when ocean resolution increases from 1° to 0.25°, both across the
166 Bering Strait (83 km wide) and through the Nordic Seas establishing the Atlantic warm inflow into the Arctic Ocean.
167 Similarly, as for SIT, the effect of the atmospheric grid resolution on the sea ice extent is model-dependent. When it is
168 enhanced, there are no notable changes in the location of the March ice edge in the ECMWF-IFS and HadGEM3 models,
169 while it is largely overestimated in CMCC-CM2 and MPI-ESM, particularly in the Nordic Seas. Specifically, CMCC-CM2

HR4 underestimates March sea ice coverage in the northern Barents Sea, the Bering Sea, and the Sea of Okhotsk, whereas the VHR4 version (with a finer atmospheric grid) reproduces a reasonable amount of winter ice in marginal seas. In September, higher atmosphere resolution leads to a larger SIA in ECMWF-IFS and CMCC-CM2, conversely it has an opposite effect in HadGEM3 and MPI-ESM models. In addition, MPI-ESM XR does significantly melt sea ice in the Siberian seas which are almost ice-free in summer. The width of the MIZ (marked in Figure 2 by the area capped between 15% and 80% SIC contours) also varies among different models. In many of them, March MIZ similarly surrounds the inner ice pack, comparing well with CDR. In September, most models fairly simulate an extension of MIZ comparable to the observed one. Exceptions are MPI-ESM runs that lose all consolidated pack ice in summer and ECMWF LR that tends to overestimate the total and pack ice, with a small portion covered by marginal ice in the Barents Sea and Nordic Seas.

3.2 Seasonal variability

Figure 3 shows the mean seasonal cycle of the total Arctic SIA and SIV computed over the 1979-2014 period. Satellite estimates from both OSISAF and CDR are included to validate the models' outputs. The CDR Arctic ice area expands to its maximum in March, with coverage of nearly 14×10^6 km^2, and returns to its minimum in September at around 6×10^6 km^2. Similar seasonality is displayed by the OSISAF dataset, which has just a slightly smaller SIA in all months.
As in CMIP5 and CMIP6 low-resolution models (Shu et al., 2020, Notz and SIMIP Community, 2020), most HighResMIP models adequately reproduce the mean seasonal cycle of SIA with the melt season starting in March and lasting until September where a minimum is reached (Figure 3a). There is a considerable spread among models, it is relatively larger in winter than in summer. March SIA ranges from 12 to 20×10^6 km^2, while September values lie in the range between 3 and 7.5×10^6 km^2 in all but one model. The ECMWF-ISF LR overestimates the Arctic SIA all year round, but it can properly represent the amplitude of SIA seasonal variability and hence correctly reproduces the ice advance and retreat phases. The comparison between the model configurations indicates that finer resolution generally results in simulated SIA closer to satellite products. The effect of changing atmosphere resolution varies among models, though. For instance, the CMCC-CM2 HR constantly stays in the lower bound of the model ensemble and reproduces a weaker amplitude of the seasonal cycle compared to observations; applying the atmospheric grid refinement (CMCC-CM2 VHR4 configuration) favourably increases sea ice coverage and does not significantly change the seasonal cycle amplitude. Different impact is observed for the MPI-ESM model: the finer atmospheric grid leads to closer agreement with observations in SIA during winter but increases the spring/summer melting resulting in an underestimated September minimum up to ~50% compared to observations. In general, in other HighResMIP runs, the atmosphere grid refinement gives smaller changes to Arctic sea ice coverage compared to the ocean resolution enhancement. In the ECMWF-IFS, the LR shows a constant SIA overestimation, that is largely resolved in the model configuration with an eddy-permitting ocean (HR), particularly in summer. The same behaviour is seen for six ECMWF ensemble members (Figure S1). As for the CMCC-CM2 model, a further refinement in the atmosphere resolution increases the SIA in the whole year with the best agreement with observation from October to July. The HadGEM3 runs are relatively close to observations in summer but they tend to overestimate the sea ice growth -

203 the impact of increased ocean and atmosphere resolution is evident for this model with a strong reduction of winter sea ice of
204 ~25% from LL to HM and a smaller but still remarkable contraction in summer. Here, the increase in the atmosphere
205 resolution further reduces SIA in contrast to previous models. Finally, EC-Earth3P and CNRM-CM6 models show negligible
206 differences between model configurations, despite ocean and atmosphere grids resolution.

207   In our reference product, PIOMAS, the Arctic SIV ranges from ~25×10^3 km^3 at its peak in April to ~10×10^3 km^3 at
208 its minimum in August/September (Figure 3b). All models capture the timing of the SIV maximum in April and the
209 minimum in August/September with a realistic seasonal cycle amplitude that ranges between 15 and 20×10^3 km^3. However,
210 there is a large spread among different models, with most models overestimating PIOMAS - ECMWF-ISF LR is a clear
211 "outlier" exceeding 70×10^3 km^3 in April and 50×10^3 km^3 in September. Although in some models the bias in SIA is
212 seasonally dependent with larger errors in winter, bias in simulated SIV is consistent throughout the year in all models. In
213 general, large SIV is mainly due to poorly simulated SIT rather than incorrect sea ice cover (Figure 2, 3a). Only in
214 ECMWF-IFS LR, the combination of large ice expansion and extremely thick ice leads to unrealistically high SIV. The SIV
215 overestimation in the CMCC-CM2 and EC-Earth3P models is caused by too thick sea ice, even though their SIA compare
216 well with observations. Only one model (CNRM-CM6 in both configurations) has thin ice and hence low bias in SIV
217 compared to PIOMAS, all year round. The changes in resolution have no visible impact in this case. The increase of only
218 ocean resolution largely improves the representation of SIV (as for SIA) in ECMWF-IFS with a large volume reduction
219 (including six ensemble members; Figure S1), but does not affect the volume seasonality in HadGEM3. Finer atmosphere
220 resolution and the combined resolution increase tend to increase the ice volume except in HadGEM3 and MPI-ESM.
221 MPI-ESM has a good fit to PIOMAS for SIV although this model underestimates SIA and cannot simulate consolidated pack
222 ice (SIC > 80%, Figure 2).

223   In addition to the total SIA, we show the seasonal variability of the area covered by marginal ice over the same
224 1979-2014 period (Figure 4a). It is worth noting that the evaluation of the simulated MIZ area is highly dependent on the
225 reference product used, particularly in summer This can be mainly ascribed to the treatment of the wet surface (e.g. melt
226 ponds, snow wetness) that poses difficulty to retrieve the SIC using passive microwave radiometers (Ivanova et al., 2015).
227 OSISAF has a small portion of MIZ in winter, while it overestimates CDR from May to November. The maximum difference
228 between the two products is up to nearly 0.9×10^6 km^2 in July. The observed MIZ seasonal variability contrasts with that
229 shown by the total ice area: the MIZ expands in spring when the consolidated pack ice starts to melt, and this process leads
230 to the MIZ area peak occurring in summer. After reaching its maximum in July, the marginal ice starts to melt and its area
231 decreases until September, simultaneously with the total and the consolidated pack ice cover. Before next year's melting
232 season, the MIZ stays relatively stable but with a secondary peak in October, at the beginning of sea ice advance. The models
233 are overall able to simulate the seasonal cycle, reasonably capturing the phases of the MIZ expansion and retreat. However,
234 they tend to overestimate the MIZ in winter, but most of them lie between the OSISAF and CDR summer estimates.
235 Generally, models struggle to properly simulate the timing and magnitude of the MIZ maximum: ECMWF-IFS LR is higher
236 than observations from November to May due to a large overestimation of the total ice area, nevertheless it lies between

CDR and OSISAF in the rest of the year. Noteworthy, the ECMWF-IFS finer resolution configurations are in better agreement with observed values. In the HadGEM3 LL configuration, the marginal ice expansion starts earlier, with a large bias of the MIZ area from March to June. Increasing resolution in HadGEM3 model does not have a visible impact for the rest of the year. The impact of changes in the ocean and atmosphere resolution is small for other models. Finally, MPI-ESM configurations fail to reproduce the MIZ seasonal cycle from June to November. This pairs with Figure 2, which shows underestimation of consolidated pack ice and MIZ predominance in the MPI-ESM runs.

We also show the seasonal cycle of the MIZ area fraction (MIZF) from 1979 to 2014, calculated from the model and satellite products outputs (Figure 4b). The MIZF is defined as the percentage of the ice cover that is MIZ (Horvat, 2021) and reflects the relative changes of the MIZ, which are highlighted since the total ice experiences substantial seasonal variability. The observed MIZF ranges from 5-10% in winter to 20-40% at its maximum between June/July. For all models, the simulated MIZF maxima are delayed compared to the satellite estimates and the MIZ area by about one month, when the total ice area approaches the September minimum and the MIZ area is still large. Notably, the HighResMIP models are in better agreement with observations when considering the MIZF rather than the MIZ area. Excluding the MPI-ESM configurations, all models are in general agreement from November to May; the model spread enlarges in spring/summer but the models lie anyway within the observation envelope. The use of the MIZF metric highlights the peculiar representation of Arctic sea ice in the MPI-ESM: up to 95% of sea ice in the model consists of marginal ice.

3.3 Seasonal variability in the sub-regions

Since sea ice changes in the Arctic region are not uniform in space and time as a result of local climate effects (cf. Parkinson et al 1999; Meier et al 2007, Peng and Meier 2018), it is important to monitor the sea ice change also on regional scales. We analyse the seasonal variability of SIA and SIV in six sub-regions and we compare it with that of reference products (Figure 5, Table 2).

Satellite estimates of SIA are not shown in the Central Arctic sector (CA) due to the observation gap near the North Pole. In this region, all models simulate a pronounced seasonal cycle in SIA with the widest area between December and April, and a minimum in August. Although most models agree in winter when the region is fully covered by sea ice, the inter-model spread increases in summer. HadGEM3 and CMCC-CM2 simulate similar seasonal cycles in all configurations with slightly lower values in HadGEM3 HM. The ECMWF-IFS LR is an outlier also in this region, with a large SIA all year round and a minimum in August that is as large as the autumn/winter values in other models. Also EC-Earth3P LR has SIA comparable to ECMWF-IFS LR from November to May, however it overestimates the melting and growing phases with an August minimum comparable to other models. The CNRM-CM6 model produces the smallest seasonal cycle amplitude in both resolutions, with a decrease between the winter values and the minimum of ~10%. On the contrary, both MPI-ESM configurations display the strongest seasonal cycle, with the largest area in winter and the smallest in summer. These differences among models do not clearly depend on the resolution changes. For SIV, PIOMAS shows an increase of ~30% between the minimum in August/September and the maximum in May. The seasonal cycle magnitude is captured by most

270 models but with a large spread mainly driven by differences in the simulated thickness (Figure 2). The models generally
271 perform similarly in simulating the SIV seasonal cycle in the sub-regions as at the hemispheric scale (Figure 3b). For the
272 sake of conciseness, only the specific features of the SIV representation at the regional scale will be indicated below. The
273 Barents-Kara Seas (B-K) is the only sub-region where satellite products show a distinct maximum peak that occurs in April
274 (one month after the hemispheric SIA maximum), cf. Figure 5a. Except for CMCC-CM2, the models generally overestimate
275 SIA in winter with a large spread among them which reduces in summer, when models are in closer agreement with satellite
276 estimates. The strong underestimation of SIA in the CMCC-CM2 HR4 configuration could be attributed to the increased
277 poleward Atlantic OHT simulated by this model (Docquier et al., 2020). The warmer ocean temperatures not only promote
278 sea ice melting in winter but also hinder its growth in autumn. The ocean and atmosphere spatial resolution have generally
279 the opposite effects on simulated SIA. Increasing only the ocean resolution in ECMWF-IFS (from LR to MR) and
280 HadGEM3 (from LL to MM) results in lower SIA and a better fit to the observations. Conversely, increasing the atmosphere
281 resolution generally leads to larger SIA, except for a decrease in SIA for HadGEM3. The combined effect of enhanced
282 resolution in both ocean and atmosphere in CNRM-CM6 and EC-Earth3P models increases the winter SIA, worsening the
283 comparison with the observations. For SIV, nearly half of the model ensemble is within the 15% of PIOMAS seasonal
284 variability from January to June which is not the case for other sectors. The Barents-Kara Seas is the only region where
285 CMCC-CM2 HR underestimates SIV as a result of too low SIA. In addition, both configurations of CMCC-CM2
286 underestimate the seasonal variation of SIV. At the same time, CNRM-CM6 better fits to PIOMAS SIV in the Barents-Kara
287 Sea sector compared to the other parts of the Arctic Ocean. The increased ocean resolution has a clear positive effect on SIV
288 representation in ECMWF-IFS configurations, whereas other models display similar values when changing such parameter.
289 On the other hand, the enhanced atmosphere resolution leads to higher SIV for ECMWF-IFS and CMCC-CM2, lower SIV
290 for HadGEM3 and does not affect SIV in MPI-ESM.

291   The Laptev (LV), East Siberian (ESS), and Beaufort-Chukchi Seas (B-C) show similar behaviour in SIA and SIV.
292 They can be analysed together and grouped as in Peng and Meier (2018). In these regions, there is no noticeable peak in the
293 observed seasonal variability of SIA, instead the annual maximum is extended between December and May since the winter
294 sea ice expansion is constrained by land. In spring, the downward shortwave radiation increases, causing the rapid sea ice
295 melt, which ends in September. Notably, the disagreement between satellite estimates in summer SIA is higher in all three
296 regions probably due to the enhanced presence of melt ponds, which complicate the SIC retrievals from passive microwave
297 radiometers (Ivanova et al., 2015). The models exhibit better agreement in winter, while the spread across models is larger in
298 summer. This could be possibly associated with the model differences in simulating atmospheric circulation, as well as the
299 river discharge (Park et al., 2020) and the transport of Pacific waters through the Bering Strait (Watts et al., 2021), which
300 modify the thermo-haline structure of the upper-ocean and affect sea ice growth and melt. In all three regions, SIA from
301 ECMWF-IFS LR is well compared with satellite estimates in winter, which is not the case for other sectors with a greater
302 role of the Atlantic OHT where the model is biased high. HadGEM3 overestimates SIA, particularly in its lower resolution
303 configuration. This behaviour is common also for other parts of the Arctic Ocean which points out that bias in HadGEM3 is

similarly distributed across the regions. MPI-ESM underestimates SIA to a greater degree in summer since the model is struggling to simulate consolidated pack ice (Figure 2). CNRM-CM6, CMCC-CM2 and HR of EC-Earth3P show a fairly good agreement with satellite estimates in all three regions. Lower resolution configuration of EC-Earth3P displays an earlier and faster sea ice retreat in the Laptev and East Siberian Seas resulting in the second-lowest SIA, while the model compares well with OSISAF estimates in the Beaufort-Chukchi Seas. Increased ocean resolution leads to lower SIA for all models except for EC-Earth3P which has higher values in its HR configuration. The effect of the ocean resolution is stronger in summer, however the impact is substantial all year round for HadGEM3. Enhancement of the atmosphere resolution does not significantly affect ECMWF-IFS but leads to higher summer SIA in CMCC-CM2, as in the other regions. For MPI-ESM, the increase in atmosphere resolution has a larger impact on summer SIA in the Laptev, East Siberian, and Beaufort-Chukchi Seas compared to other sectors: MPI-ESM XR simulates SIA almost twice lower than CDR in August and September. In the Laptev, East Siberian, and Beaufort-Chukchi Seas, SIV reaches the maximum in May (April-May in B-C) while the annual minimum occurs in September. Most models overestimate SIV with the highest bias (ECMWF LR) in the East Siberian and Beaufort-Chukchi Seas. CMCC-CM2 HR and MPI-ESM HR are the closest to PIOMAS, even though the latter fails to reasonably simulate the SIC (Figure 2). The effect of the ocean resolution on SIV is clearly seen for ECMWF-IFS and EC-Earth3P in all three regions and for HadGEM3 in the Laptev Sea - the only region where LL and MM configurations of HadGEM3 differ. Other models do not show considerable differences in SIV when changing ocean resolution. Finally, increased atmosphere resolution results in higher SIV for ECMWF-IFS, EC-Earth3P, and CMCC-CM2 and lower SIV for HadGEM3 and MPI-ESM.

The Greenland region (GD) holds the largest area of sea ice both in winter and summer (3 and 1.5×10^6 km^2 respectively according to the satellite estimates). Most models tend to overestimate SIA all year round with the highest bias in winter in ECMWF-IFS LR and HadGEM3. The models are generally capable of melting away the excess of sea ice by August, so there is more consistency among most models in summer, when MPI-ESM underestimates SIA more than all of them. An increase in the ocean resolution from 1° to 0.25° effectively improves the representation of SIA in ECMWF-IFS, whereas it does not give notable changes in HadGEM3 and EC-Earth3P. The effect of atmosphere resolution again depends on the model. ECMWF-IFS and CMCC-CM2 display slightly higher SIA in their finer atmosphere configurations, particularly in winter. Conversely, HadGEM3 has lower SIA in its HM configuration in winter, which fits better to the observations. For MPI-ESM, there are no differences between different configurations, as in the Barents-Kara Seas region. For SIV, both configurations of CMCC-CM2 have a large error in the Greenland region owing to high bias in SIT (Figure 2); whilst at least one configuration of the model is in good agreement with PIOMAS in other sectors. Enhanced ocean resolution leads to lower SIV for ECMWF-IFS and higher SIV for EC-Earth3P. At the same time, there are no significant differences between configurations of HadGEM3 and CNRM-CM6 with changing ocean resolution. An increase in the atmosphere resolution has almost no effect on SIV in HadGEM3 and MPI-ESM but leads to higher SIV in CMCC-CM2

The displayed analysis reveals that the model performance and the accuracy of simulated SIA largely depend on the Arctic region and the season studied. While the Barents-Kara Seas and Greenland regions contribute mainly to the winter

338 inter-model spread, the largest summer differences among models are seen in the Laptev, East Siberian and
339 Beaufort-Chukchi Seas. There are no considerable differences in the model ability to simulate SIV at the regional scale, in
340 fact the biases are generally uniform across regions and seasons. Generally, we find no strong dependence of sea ice realism
341 from the horizontal resolution. The impact of the ocean resolution on the representation of SIA is most pronounced in the
342 Barents-Kara Seas and Greenland sea ice regions that are strongly influenced by the Atlantic OHT. The effect of the
343 atmosphere resolution is less clear but there is evidence that the atmosphere resolution has a stronger impact on SIV rather
344 than on SIA and particularly in the regions of thicker ice (B-C, GD).

345

346 Table 2. March and September SIA for each region (except CA) in each model for 1979-2014.

	March (10^6 km^2)					September (10^6 km^2)				
	BK	LV	ESS	B-C	GD	BK	LV	ESS	B-C	GD
ECMWF-IFR LR	3.06	1.1	1.57	2.16	4.05	1.87	0.84	1.41	1.73	3
ECMWF-IFR MR	2.12	1.08	1.56	2.15	3.22	0.62	0.57	1.19	1.56	1.45
ECMWF-IFR HR	2.46	1.09	1.56	2.14	3.53	1.06	0.64	1.25	1.61	1.7
EC-Earth3P	2.13	1.11	1.58	2.18	3.17	0.45	0.35	0.74	1.26	1.56
EC-Earth3P HR	2.43	1.1	1.57	2.17	3.32	0.72	0.52	1.06	1.56	1.43
CNRM	2.39	1.11	1.58	2.19	3.43	0.76	0.66	0.68	1.12	1.26
CNRM HR	2.64	1.1	1.57	2.17	3.35	0.6	0.47	0.8	1.2	1.08
HadGEM3 LR	2.89	1.31	1.85	2.31	4.29	0.78	0.71	1.22	1.45	1.8
HadGEM3 MM	2.7	1.23	1.68	2.3	4.41	0.79	0.6	1.17	1.59	1.68
HadGEM3 HM	2.38	1.17	1.63	2.24	3.84	0.4	0.43	0.95	1.46	1.45
CMCC-CM2 HR	1.4	1.1	1.56	2.13	2.9	0.22	0.47	0.68	1.05	1.41
CMCC-CM2 VHR	1.98	1.11	1.57	2.15	3.25	0.66	0.63	1	1.44	1.76
MPI-ESM HR	2.31	1.03	1.52	2.1	2.93	0.42	0.38	0.68	0.95	0.72

MPI-ESM XR	2.48	1.04	1.53	2.11	3.39	0.37	0.24	0.36	0.62	0.65
CDR	2.19	1.11	1.58	2.18	3.07	0.64	0.54	0.9	1.28	1.38
OSISAF	2.09	1.11	1.57	2.15	2.97	0.56	0.48	0.8	1.17	1.28

347

3.4 Interannual variability and trends

349   Next, we evaluate the long-term variability of the Arctic SIA and SIV from the hist-1950 simulations from 1979 to
350 2014. Figure 6a illustrates monthly anomalies of SIA (with respect to 1979-2014 climatologies) simulated by the models and
351 derived from satellite data sets. The inter-model spread is relatively similar throughout the period but it increases from the
352 mid-2000s when the ice reduction has accelerated. All models are able to reproduce the sea ice shrinking but with varying
353 intensity: ECMWF-IFS LR, HadGEM3 LL, MPI-ESM HR show larger negative trends compared to observations (-44x10^3
354 km^2 yr^{-1} in CDR and -46x10^3 km^2 yr^{-1} in OSISAF), while the MR and HR versions of ECMWF-IFS, both configurations of
355 CNRM-CM6, EC-Earth3P, HadGEM3 HM, and CMCC-CM2 HR display weaker negative trends (Table 3). An increase in
356 the ocean resolution generally results in smaller negative trends except for EC-Earth3P which shows a similar decline rate in
357 both configurations. Note that weaker trends are also observed in six HR ensemble members of ECMWF-IFR in comparison
358 to their low-resolution counterparts (Table S1). The effect of finer atmosphere resolution is different among models: the SIA
359 decrease is stronger in ECMWF-IFS and CMCC-CM2 and weaker in HadGEM3 and MPI-ESM.

360   Figure 6b shows monthly anomalies of SIV (with the seasonal cycle removed) over 1979-2014 in HighResMIP
361 models and PIOMAS. There is a substantial inter-model spread for SIV compared to SIA, particularly at the beginning and
362 the end of the observed period (55-85% of yearly averaged SIV from PIOMAS). The biases from a few models are not
363 consistent throughout the years varying significantly from positive to negative (EC Earth-3P HR, ECMWF MR, HadGEM3
364 LL).

365   PIOMAS simulates sea ice shrinking at the rate of -291 km^3 yr^{-1}; similarly, all models simulate a SIV decrease.
366 There is no straightforward impact of changing resolution in the ocean and atmosphere on the linear trends in SIV since the
367 impact of horizontal resolution on SIA and SIT differs from the models. However, we find that configurations with coarse
368 ocean resolution generally tend to simulate more negative trends (-424 km^3 yr^{-1} in ECMWF LR compared to -105 and -157
369 km^3 yr^{-1} in its finer configurations; for HadGEM3, the trend ranges from -355 km^{3}yr^{-1} in lower resolution to -257 and -174
370 km^3 yr^{-1} in finer resolution configurations). We observe the same for the ECMWF ensemble members (Table S1). Here, the
371 exception is EC-Earth3P in which the eddy-permitting configuration has a larger negative trend in SIV (-322 and -460 km^3
372 yr^{-1}). This might be attributed to the thicker ice simulated in the HR configuration (Figure 2). In CNRM-CM6, the SIV
373 decrease is very weak (-62 and -36 km^3 yr^{-1} for LR and HR configurations, respectively), which might reflect the negative
374 ice growth-ice thickness feedback: thin ice allows sea ice to grow more rapidly mitigating the ice loss. The finer atmosphere
375 resolution has a different impact on the pace of sea ice retreat in different models: CMCC-CM2, VHR4 and ECMWF-IFS
376 HR simulate slightly stronger trends compared to their coarser counterparts (-384 km^3 yr^{-1} and -411 km^3 yr^{-1} in CMCC-CM2;

13

377 -105 and -158 km^3 yr^{-1} in ECMWF-IFS). On the other hand, in MPI-ESM and HadGEM3, the finer configuration has less

378 negative trend compared to the coarser one (-337 km^3 yr^{-1} and -144 km^3 yr^{-1} in MPI-ESM; -174 and -257 km^3 yr^{-1} in

379 HadGEM3).

380   We also examine how the models simulate sea ice response to the external forcing on a seasonal scale. The monthly

381 trends in the Arctic-wide SIA (computed over the period 1979-2014) reveal that the models tend to underestimate the rate of

382 sea ice loss in the melting season and in summer (not shown). Most models reproduce more negative trends from November

383 to May and underestimate the magnitude of trends in other seasons. MPI-ESM HR trends are found to have a closer fit to the

384 observed trends for the total Arctic although the model is wrong in simulating SIC and sea ice classes. For SIV, the models

385 vary greatly in the representation of trends. Despite all models being able to simulate a SIV decline in all months, they

386 cannot capture the observed magnitude of sea ice loss and have values ranging from almost 0 to -450 km^3 yr^{-1}. They also

387 struggle to reproduce the seasonal cycle in the trend which in PIOMAS has a slightly stronger signal in June and a weaker

388 signal in the winter months (-320 km^3 yr^{-1} and -260 km^3 yr^{-1} respectively).

389

390 **Table 3. Linear trend in SIA and SIV and their standard deviations for 1979-2014 and 2015-2050 periods.**

	1979-2014 SIA trend (10^3 km^2/yr)	2015-2050 SIA trend (10^3 km^2/yr)	1979-2014 SIV trend (km^3/yr)	2015-2050 SIV trend (km^3/yr)
ECMWF-IFR LR	-72.08 ± 16.9	No future runs	-423.86 ± 68.3	No future runs
ECMWF-IFR MR	-21.24 ± 9.8		-104.82 ± 71.4	
ECMWF-IFR HR	-36.67 ± 7.6		-157.58 ± 34.4	
EC-Earth3P	-34.2 ± 9.47	-52.31 ± 16.1	-322.28 ± 31.8	-210.56 ± 64.1
EC-Earth3P HR	-40.13 ± 8.8	-54.87 ± 5.5	-460.47 ± 97.5	-368.47 ± 31.7
CNRM	-29.83 ± 8.9	-6.55 ± 13.4	-61.89 ± 23.6	-35.55 ± 26.7
CNRM HR	-15.94 ± 7.9	-63.9 ± 9.2	-35.58 ± 15.9	-131.21 ± 20.5
HadGEM3 LR	-56.54 ± 13.1	-113.91 ± 12.5	-354.64 ± 66.2	-361.87 ± 31.7
HadGEM3 MM	-48.32 ± 10.8	-97.68 ± 11.3	-256.75 ± 41.2	-459.86 ± 36.7
HadGEM3 HM	-31.54 ± 8.3	-106.72 ± 10.2	-173.72 ± 38.5	-440.09 ± 52.6
CMCC-CM2 HR	-38.57 ± 5.2	-47.55 ± 9.7	-384.2 ± 30.9	-286.38 ± 31.2
CMCC-CM2 VHR	-40.83 ± 6.6	-73.97 ± 6.6	-411.1 ± 51.1	-698.79 ± 37.5
MPI-ESM HR	-52.19 ± 5.1	-49.94 ± 8.3	-336.95 ± 22.8	-116.95 ± 19.7

MPI-ESM XR	-36.94 ± 9.5	-46.95 ± 8.5	-143.97 ±44.5	-99.39 ± 16.4
CDR	-44.14 ± 7.3			
OSISAF	-46.42 ± 6.7			
PIOMAS			-291.27 ± 36.8	

Since there is a substantial difference in the models' performance in reproducing the seasonal variability on a regional scale, we analyse monthly trends in SIA and SIV in each sea ice zone over 1979-2014 (Figure 7). The magnitude and timing of sea ice loss strongly depend on season and region. According to observations, the winter decrease in SIA is most dramatic in the Barents-Kara Seas (nearly -17x10^3 km^2 yr^{-1}; 0.8% yr^{-1}) while the summer trends are dominated by the Eastern Siberian Sea and Beaufort, and Chukchi Seas (almost -25x10^3 km^2 yr^{-1}; 2-3% yr^{-1}). The Barents-Kara Seas and the Greenland region show a pattern of SIA trends that differs from the total Arctic and the rest of the regions which have one pronounced negative peak in September and trends close to zero in winter. Instead, in the Atlantic sector, i.e. Barents-Kara seas and Greenland coast, sea ice loss is observed all year round with a slightly stronger decrease in July. In the Central Arctic, the models simulate a weak SIA reduction with the strongest signal in August-September, which is not significant in most models (less than 5% of the SIA of the sector). In the other sectors, the models generally tend to underestimate the pace of sea ice loss indicated by satellite estimates. The exception is the Barents-Kara Seas and Greenland where some models produce more negative trends compared to the observations. In the Laptev, East Siberian, and Beaufort and Chukchi Seas some of the models do not simulate a reduction in summer SIA and even display weak positive trends, yet insignificant. Given that all these regions hold a large MIZF in summer (Figure 4), the inability to capture trends points to inaccurate sensitivity of sea ice to the external forcing, particularly within the MIZ.

The strongest negative trends in SIV are observed in the areas of thick ice: the Beaufort and Chukchi Seas (up to -90 km^3 yr^{-1} in September), the Greenland sector (-80 km^3 yr^{-1} in July), and the East Siberian Sea (-70 km^3 yr^{-1} in summer months). The seasonal cycle of the Barents-Kara Sea SIV trend contrasts with those of other sectors where the highest rate of sea ice decline is observed in September. Notably, in the Laptev, East Siberian, and Beaufort and Chukchi Seas, SIV experiences a substantial decrease in the winter months while SIA stays nearly stable reflecting a considerable ice thinning primarily driven by basal melting. In the East Siberian Sea and Beaufort-Chukchi Seas, almost all models tend to underestimate trends in SIV (10 out of 14 model simulations produce less negative trends) while in the rest of the Arctic zones, PIOMAS is nearly in the middle of inter-model spread. Compared to other models, both CNRM-CM6 configurations and the two finest configurations of ECMWF-IFS have changes in SIA and SIV closer to zero in almost all regions and months. On the one hand, CNRM-CM6 simulates very thin ice so the lack of trend is consistent with the concept of negative ice thickness-ice growth feedback. On the other hand, ECMWF-IFS MR and HR underestimate sea ice reduction everywhere despite simulating very thick ice. HadGEM3 performs differently at regional scale but at least one of the configurations has a

420 very good fit to the PIOMAS estimates. Generally, both configurations of CMCC-CM2 present the large SIV decrease in all
421 sectors except for the Barents-Kara Sea and the rate of decline is similar between two resolutions despite a significant
422 difference in the mean SIV. The HR configuration of MPI-ESM is in fairly good agreement with PIOMAS in all regions
423 except the Central Arctic and the Laptev Sea where it tends to produce more negative trends. Conversely, MPI-ESM XR
424 underestimates negative SIV trends in all parts of the Arctic Ocean except the Greenland zone where it is close to its HR
425 configuration.

426   Overall, there is no consistent link between the strength of sea ice retreat and the ocean/atmosphere resolution, it
427 rather depends on the region and the model used. Considering only SIA, the models generally underestimate the trends
428 especially in finer ocean configurations and in Laptev, East Siberian and Beaufort and Chukchi Seas in summer. However,
429 beneficial effects of increased ocean resolution for SIA trends are observed for ECMWF-IFS in the Barents-Kara Seas and
430 the Greenland area. In these regions, other models do not considerably differ between configurations; low and
431 high-resolution configurations show closer fit to the observations according to the season. Moreover, the increased
432 atmosphere resolution also does not improve the representation of SIA trends; HadGEM3, CMCC-CM2 and MPI-ESM finer
433 atmosphere configurations lead to underestimating the negative SIA trends more than their counterparts at coarse resolution.
434 The relation between ocean/atmosphere resolution and SIV trends is less clear and depends on the region and the model.

435 **3.5 Future projections**

436 In this section, we analyse the results of HighResMIP models when simulating future Arctic sea ice changes using
437 highres-future model outputs from 2015 up to 2050. HighResMIP future projections generally show a stronger sea ice loss
438 compared to historical runs (Table 3). These simulations can elucidate when the Arctic will reach its first "ice-free" summer,
439 i.e. the condition typically defined as the timing when September sea ice drops below 10^6 km^2. Reaching ice-free conditions
440 is an unprecedented change in the Arctic environment and the tipping-point in the Earth's climate system. Considering the
441 large inter-model spread in simulating observed mean sea ice state and trends, we assume that a selection of the models
442 which better agree with observations can reduce the spread and decrease uncertainty in the model projections. We select
443 models based on their historical performance of September SIA and SIV mean state and trends against CDR and PIOMAS,
444 respectively (Figure 8). To exclude outliers, we define the 75th percentile threshold and we select the models whose values
445 do not exceed the threshold for both variables. The resulting subset includes four models: low-resolution configuration of
446 EC-Earth3P, HadGEM3 MM and HM, and CMCC-CM2 HR. These models are used in the further analysis on sea ice future
447 evolution.

448   Figure 9 illustrates the September SIV time series from 1950 to 2050 computed for total Arctic and sub-regions.
449 The vertical lines mark first ice-free September in the multi-model mean with and without model selection (yellow and
450 green, respectively) and in CDR (black, data available between 1971-2021). At the regional scale, the timing of ice-free
451 conditions refers to the threshold of 25% of the CDR SIA averaged over the 1980-2010 period in the given region. It is
452 evident that huge sea ice reduction takes place in all Arctic sectors, however the pace of sea ice loss varies across the regions
453 owing to differences in the initial state and dominant processes driving the change. We can note that applying model

16

454 selection results in earlier timing of the ice-free conditions in Barents-Kara, Laptev, East Siberian, and Beaufort-Chukchi
455 Seas and in ice-free conditions in the total Arctic, Central Arctic, and Greenland region. In latter sub-regions, multi-model
456 mean without model selection does not predict the event everywhere before 2050. The comparison between the model
457 configurations in simulating timing of ice-free conditions shows that there is no clear link between the model resolution and
458 the pace of sea ice loss (not shown).

459 The September Arctic-wide sea ice from the multi-model mean (with model selection) shrinks by 95% from 1950 to 2050,
460 cf. top panel of Figure 9. The inter-model spread decreases throughout the century from $14x10^3$ in 1950 to $1.64x10^3$ km^3 in
461 2050. The Arctic does not reach the ice-free conditions within 2050 in the multi-model mean without model selection,
462 although applying selection criteria advances the timing of the event up to 2047. The Central Arctic September sea ice will
463 lose 96% of its volume by 2050 in the multi-model ensemble, which is in good agreement with PIOMAS in the overlapping
464 period. The inter-model spread again narrows substantially from $2.58x10^3$ km^3 in 1950 to $0.23x10^3$ km^3 in 2050. The ice-free
465 conditions in the Central Arctic are not reached before 2050 in the multi-model mean when considering all models.
466 However, outliers' exclusion leads to approaching the threshold in 2042. The Barents-Kara Seas experiences the most
467 dramatic sea ice loss accounting for almost 100% of SIV from 1950 to 2050 in the models' ensemble. The first ice-free
468 September in the Barents-Kara Seas is accurately simulated by the multi-model mean with model selection: the event occurs
469 in 2012 as for CDR. Avoiding model selection postpones the event by 19 years. In the Barents-Kara Seas, the spread among
470 models is decreasing from $1.46x10^3$ km^3 in 1950 to almost vanishing in 2050. The multi-model mean SIV in the Laptev Sea
471 shrinks by 99% during 100 years. The inter-model spread narrows from nearly $0.9x10^3$ km^3 at the beginning of the run to
472 $0.05x10^3$ km^3 in the end. The timing of the first ice-free summer is similar to that in the Barents-Kara Seas: SIA drops below
473 the threshold in 2012 for CDR and in 2032 for the multi-model mean without model selection. When applying selection
474 criteria, the ice-free conditions are reached in 2023. In the East Siberian Sea, September ensemble-mean SIV is reduced by
475 99% by the middle of this century. The East Siberian Sea reaches the threshold in SIA earlier compared to the other regions.
476 CDR produces the event in 2007, when the Arctic broke the first record low while the multi-model mean with model
477 selection simulates the first ice-free conditions in 2033 (2034 without model selection). The inter-model spread ranges
478 between $4.76x10^3$ km^3 in 1950 and $0.1x10^3$ km^3 in 2050. The Beaufort-Chukchi Seas lose nearly 96% of SIV in 100 years in
479 the ensemble mean. The inter-model spread decreases from $3.44x10^3$ km^3 at the beginning to $0.37x10^3$ km^3 at the end of the
480 run. The multi-model mean reaches the first ice-free September in 2046. When adopting the model selection, the
481 Beaufort-Chukchi Seas will be ice-free in 2039. The Greenland region is undergoing the least prominent sea ice loss
482 accounting for 88% throughout the period from 1950 to 2050. However, there is a great narrowing of the inter-model spread
483 from $6.12x10^3$ km^3 in the middle of the last century to $1.15x10^3$ km^3 100 years after. Both multi-model means project that
484 Greenland SIA might turn ice-free in 2048. Overall, the models simulate the first ice-free September later than CDR in all
485 sub-regions studied. Therefore, we can fairly assume the same behaviour for the Total Arctic

486 Along with overall sea ice loss, there are substantial changes in the structure of sea ice cover. Figure 10 shows the
487 time series of September SIA and the MIZF from 1950 to 2050. For SIA (top panel), the models are in fairly good agreement

17

with the observations, yet have systematic biases and underestimate the negative trend. In addition, the inter-model spread is large but relatively similar throughout the years (~4x10^6 km^2). For the MIZF (bottom panel), the spread among models increases considerably with time from ~10% in 1950 to ~75% in 2050. Most models simulate the MIZF growth, which reflects the transition of the sea ice state to the marginal ice-dominated. The MIZ in the 2040s is projected to account for up to 80% of the total ice area in September, although the interannual variability at the end of the run is large in most models. CNRM-CM6 and MPI-ESM models are two outliers: CNRM-CM6 has a nearly constant MIZ fraction during the whole period, while MPI-ESM has MIZF close to 100% from the beginning of the run but it occasionally drops to 0 at the end of the run. Distinct models' performances in simulating MIZF show that an accurate representation of the total SIA does not guarantee the same for all sea ice classes, highlighting the importance of studying the Arctic MIZ.

4 Discussion

Although the latest generation of the models does a fairly reasonable job in simulating the mean state and long-term variability of sea ice cover (Notz and Community, 2020), the models still suffer from biases, which decrease the model's trustworthiness in projecting the future sea ice state in the Arctic. The enhancement in the model components' horizontal resolution is used in the CMIP6 HighResMIP as one of the factors capable of improving the realism of the model simulations and reducing biases in polar regions. In this study, we investigated the ability of HighResMIP in simulating Arctic sea ice variability and the impact of the ocean and atmosphere horizontal resolution on the representation of sea ice properties in the recent past and future climate. We do not find a strong link between ocean/atmosphere resolution and the representation of sea ice properties, and the realism of model performance rather depends on the model used. Nevertheless, there is evidence that an enhanced ocean resolution leads to an improved representation of winter SIA in some models. This is associated with a more accurate meridional heat transport (Docquier et al., 2019) which is a key process that can regulate the location of the ice edge and SIA (Li et al., 2017; Muilwijk et al., 2019). The Atlantic Ocean is the main heat source entering the Arctic, accounting for 73 TW on average per year (Smedsrud et al., 2010), therefore an adequate simulation of the boundary currents is particularly important in the Atlantic sector of the Arctic Ocean which is confirmed by the regional analysis in our study. Another process that might be sensitive to horizontal ocean resolution is the Arctic river discharge, which contributes both to seasonal variations of sea ice cover and long-term sea ice variability. The freshwater input stabilizes the upper ocean stratification and isolates the warm Atlantic layer from the bottom of the sea ice cover (Carmack et al., 2015), resulting in higher ice growth in winter. On the other hand, the heat input from the rivers accelerates sea ice melt and increases the ocean temperature, which has possible implications for the next year's growing season (Park et al., 2020). The representation of river discharge in HighResMIP models needs additional investigation. Our results do not show the systematic impact of atmosphere resolution on the representation of the Arctic sea ice. This is confirmed by other studies reporting the minor role of atmosphere resolution compared to that of the ocean (Roberts et al., 2020; Koenigk et al., 2021; Meccia et al., 2021). However, increasing atmosphere resolution might permit a more realistic representation of precipitation, which can lead to increased snowfall (Strandberg and Lind, 2021) and consequently invoke cooling and sea ice expansion (Bintanja et al., 2018).

522   SIT is less responsive to changes in the ocean grid resolution compared to SIA and its representation largely
523 depends on the sea ice model. Our results show that in some cases large biases in SIT reduce the beneficial effect of
524 increased horizontal resolution to SIA. Poor representation of SIT is a great obstacle to the robustness of sea ice projections.
525 The high uncertainty cannot be overcome without constraining the model simulations with a sufficient number of in-situ
526 measurements of the Arctic SIT, which are still sparse and unreliable (Massonnet et al., 2018). Apart from the horizontal
527 resolution, there are other important factors affecting the model performance; for example, inaccurate representations of
528 mixed layer depth (Watts et al., 2021), surface air temperature (Papalexiou et al., 2020), surface pressure and geostrophic
529 winds (Kwok and Untersteiner, 2011; Stroeve et al., 2014), and sea ice sensitivity to global warming (Zhang, 2010). These
530 elements pair with the intrinsic complexity of sea ice models that include thermodynamics schemes and parametrizations
531 (Keen et al., 2021), sea ice dynamics components (Hunke, 2010) and coupling between the ocean and atmosphere
532 components (Hunke et al., 2020). Given few improvements with increased horizontal resolution, we argue that running the
533 models at higher resolution might not be worth the major effort of costly computations. Our results suggest that the efforts of
534 the modelling groups should be aimed rather at the improvement of the sea ice model physics and parameterizations.

535   Our analysis is limited to only one ensemble member of each model configuration, which does not allow for a
536 proper assessment of the role of internal variability. It is important to emphasize that internal variability can easily lead to
537 marked differences between the basic features of the climate models. Results from large ensembles of multidecadal
538 simulations are required to robustly quantify internal climate variability and convincingly identify deficiencies and
539 demonstrate potential progress of the climate models (e.g. Deser et al., 2020; Maher et al, 2020). Large ensembles with
540 individual CMIP-class models show that the differences between ensemble members reflect simulated internal variability.
541 For Arctic sea ice, internal variability has a large influence on multi-decadal trends (e.g., Swart et al., 2015), and has
542 reinforced anthropogenic September Arctic ice loss since 1979 (Kay et al., 2011). Using a single member or small ensembles
543 to conclude that a climate model is in error can lead to inappropriate conclusions about the model fidelity. While a large
544 number of ensemble members is desirable to account for fluctuations due to internal variability, we acknowledge that these
545 are computationally expensive and may not be always available. Unfortunately, not all HighResMIP models used in this
546 study provide multiple members. ECMWF-IFR LR, MR, and HR have 8, 3, and 6 ensemble members, respectively;
547 EC-Earth3P and CNRM have 3 ensemble members for both the LR and HR systems. Only one member is available for all
548 the other configurations. In the supplementary material, we provide additional analysis of the above-mentioned models that
549 includes all existing model members to show the weakness and robustness of the single-model response. For these three
550 models, we show SIA and SIV variability on seasonal (Figures S1, S3, and S5) and interannual (Figures S2, S4 and S6)
551 timescales, and linear SIA and SIV trends (Table S1, S2 and S3) from 1979 to 2014 for ensemble members of LR and HR
552 configurations. The minimum and maximum deviation among the "control" member for each month depict the bounds of
553 simulated internal variability. The internal variability tends to be the largest in late autumn and winters and the smallest at the
554 summer sea ice minimum when the reduced ice coverage leads to relatively low variability as seen in the seasonal cycle. In
555 this case, the effect of resolution does not depend on the choice of ensemble member. The magnitude of the 36-year trends in

SIA and SIV is most affected, but with the small-ensemble mean generally comparable with the single-member results (with the exception of CNRM ice area). Still the LR area and volume exhibit stronger (weaker) negative trends than their HR counterpart in ECMWF (EC-Earth3P). It is worth noting that these very small ensembles do not offer considerably better sampling of internal climate variability than single-model ensemble. Although the correct sampling of internal variability is a necessary condition for assessing model fidelity, it is also crucial to assess how the model simulates the physical mechanisms of interest. However, our analysis highlights that large ensembles of multidecadal credible simulations along with strengthening the effort towards developing more realistic climate models are needed to understand sea ice trends.

In this study, we try to understand when the Arctic will see its first ice-free summer using HighResMIP outputs. Models show a wide temporal range for the occurrence of ice-free conditions in the Arctic. To reduce the inter-model spread in sea ice projections we apply a widely used approach based on the selection of models according to their historical performance (Wang and Overland, 2012; Sentfleben et al., 2020). Although close agreement with observations do not guarantee the realism of the models, we believe that excluding the models that struggle to reproduce present-day SIA and SIV mean state and trends might improve the accuracy of future sea ice projections. Different criteria to select "best-performing" models exist and almost always lead to earlier near-disappearance of sea ice compared to no selection (Docquier and Koenigk, 2021). The timing of the first ice-free Arctic in our model selection compares well with similar criteria applied to CMIP6 models which predict the event between 2047 and 2052 while the process-based criteria advances the timing of the first ice-free summer up to 2035 (Docquier and Koenigk, 2021). However, the investigation of model selection criteria is out of scope of this study; our goal is to give an insight into when the Arctic might turn ice-free.

Our results highlight the increasing role of the MIZ in the response of Arctic sea ice to climate change. We show that the MIZ will be the dominant sea ice class in the Arctic by 2050 which implies the shift to new sea ice conditions similar to those in Antarctica. The chaotic interannual variability of the summer MIZF in the last years of simulations points out that the current models' physics might not be suitable to changing sea ice conditions (Figure 10). In order to realistically simulate (thermo)dynamical processes, the new sea ice regime requires modifications in the models' physics and sea ice rheology which is formulated for thick pack ice (Aksenov et al., 2017). Additionally, the growing fraction of the MIZ requires changes in the parameterization of the lateral and basal melt (Smith et al., 2022). The proper simulation of MIZ is essential for achieving reasonable projections of future sea ice conditions since small and thin ice floes within the MIZ are more vulnerable to external dynamic and thermodynamic forces than consolidated pack ice. In addition, the water patches between the ice floes permit the absorption of solar radiation in the upper ocean, increasing the role of the ice-albedo effect which causes anticipation of the ice-advance onset and acceleration of the overall sea ice loss. To demonstrate positive feedback between summer MIZ and minimum SIA for the following year we plot the mean MIZF over June, July, August, and September (JJAS) against September SIA with a 1-year lag computed for the years 2015-2050 (Figure 11a). All models except one simulate negative regression ranging from ~ -0.13 %/10^6 km^2 to -0.06 %/10^6 km^2 which means that the larger summer MIZF leads to lower September SIA the following year. We suggest that the MIZ might act as a predictor of future sea ice conditions in the model simulations. Figure 12b shows JJAS MIZF in 2015 (start of highres-future run) against the

590 first September when the Arctic becomes ice-free. Note that not all models simulate the event before 2050. Our analysis
591 indicates that with the higher initial MIZF, the September sea ice disappears earlier. This points out that the reasonable
592 representation of the MIZ at the beginning of the run might impact the pace of sea ice loss and potentially improve the
593 accuracy of model projections. We assume that the MIZF might represent a robust criterion to examine the model fidelity.
594 The impact of the MIZ on the accuracy of the model simulations needs further investigation.
595

596 5 Conclusions

597   In this study, we evaluate the historical and future variability of the Arctic sea ice area and volume using six
598 coupled atmosphere-ocean general models participating in the HighResMIP experiments of the sixth phase of the Coupled
599 Model Intercomparison Project (CMIP6). For the period 1979-2014, we find that most models can properly simulate
600 maximum and minimum of the SIA seasonal cycle at hemispheric and regional scales. However, some of them cannot
601 correctly capture their magnitude, failing to realistically reproduce the ice growth and retreat phases with systematic over- or
602 underestimation of the seasonal variability. We find that the models are generally able to reproduce the seasonal cycle of the
603 Arctic-wide MIZ area, although not all of them can capture the timing of the annual maximum. The models simulate
604 different areas of the MIZ, especially in summer, however, there is stronger agreement among models for MIZF. We find
605 different regional contributions to the inter-model spread associated with seasonal variability: the winter inter-model spread
606 in SIA is attributed to the Atlantic sector (Barents-Kara Seas and the Greenland ice zones), while the summer differences are
607 tied to the the Laptev, East Siberian, and Beaufort-Chukchi Seas.
608 Selected models broadly differ on the spatial distribution of the mean SIT as well as its average values. Only few models
609 reveal a pattern similar to PIOMAS characterised by thicker ice off the coast of Greenland and the Canadian Archipelago.
610 Most models simulate too thick ice which affects the representation of sea ice volume: excluding one outlier, all but two
611 models overestimate ice volume all year round up to 1.5 times in April and 3.5 times in August. However, regardless of large
612 systematic biases, most models simulate a realistic seasonal cycle of SIV with a maximum in April and a minimum in
613 August. All models capture declines in SIA and SIV over the historical period but they disagree on the pace of sea ice loss.
614 The response to the external forcing does change with season and region: the winter trends are dominated by changes in the
615 Barents-Kara Seas and the Greenland ice zone, while the summer trends are driven by those in the East Siberian, and
616 Beaufort-Chukchi Seas. Most models underestimate ice loss in all regions particularly in summer; conversely, they tend to
617 simulate more negative trends in the Greenland zone leading to overestimating the Arctic-wide SIA trend in some
618 configurations. In this study, we find that there is no strong relationship between ocean/atmosphere resolution and sea ice
619 cover representation: the impact of horizontal resolution rather depends on the studied variable and the model used.
620 However, the ocean has a stronger effect than the atmosphere and the increase in the ocean resolution from $\sim 1°$ to $\sim 0.25°$
621 has a favourable impact on the representation of SIA and sea ice edges which is especially evident for ECMWF-IFS and
622 HadGEM3 models. At the same time, the simulation of SIT does not directly rely on the grid spacing, as well as the derived
623 SIV. A finer ocean resolution leads to lower SIV for ECMWF-IFS and to almost no differences for HadGEM3. Increasing

21

resolution both in ocean and atmosphere results in little difference between configurations in CNRM and higher SIV for EC-Earth3P. On the other hand, enhanced atmosphere resolution leads to higher SIV for ECMWF-IFS and CMCC-CM2 and lower SIV for HadGEM3 and MPI-ESM. We also find that the difference between configurations varies from one region to another which highlights the importance to examine the model performance at the regional scale. For example, CMCC-CM2 HR4 has too low SIA and SIV in the Barents Sea caused by overestimating the OHT at the Barents Sea Opening (Docquier et al., 2020) while performing well in the rest of the sectors. On the other hand, MPI-ESM has similar SIA in two configurations in the Barents-Kara Seas and the Greenland ice zone, whereas the finer atmosphere configuration displays less sea ice in summer in the rest of regions.

Considering the period 2015-2050, all models simulate a long-term decrease in SIA and SIV with a generally stronger rate of ice loss compared to the historical period. Model simulations predict that the Arctic loses nearly 95% of SIV from 1950 to 2050. There is again no systematic impact of horizontal resolution on the occurrence of first ice-free conditions. The multi-model mean of all models does not project the Arctic to become ice-free before 2050. However, applying the model selection based on historical performance advances the event up to 2047. Considering that the model selection leads to closer agreement with CDR on the year of first ice-free summer in the regions where it already happened (the East Siberian, Barents and Kara, and the Laptev Sea), we infer that model selection application may potentially improve the accuracy of model projections of Arctic sea ice evolution. Together with the overall ice shrinking, we studied the changes in the structure of sea ice cover and we concluded that the MIZ will constitute up to 60-80% of the September SIA by 2050. This suggests a shift to a new sea ice regime similar to that in the Antarctic. Given that the MIZ will play a major role in the response of the Arctic sea ice to external forcing, modifications in the model physics and parametrizations are encouraged in the new generations of coupled climate models.

Author contributions

JS analyzed the model output and observational data, and wrote the paper with contributions from all co-authors. DI conceived and designed the study. All authors provided scientific input.

Competing interests

The contact author has declared that none of the authors has any competing interests.

Acknowledgments

References

Aksenov, Y., Popova, E. E., Yool, A., Nurser, A. J., Williams, T. D., Bertino, L., and Bergh, J.: On the future navigability of Arctic sea routes: High-resolution projections of the Arctic Ocean and sea ice, Marine Policy, 75, 300–317,

659 doi:10.1016/J.MARPOL.2015.12.027, 2017.

660 Ärthun, M., Onarheim, I. H., Dörr, J., and Eldevik, T.: The Seasonal and Regional Transition to an Ice-Free Arctic,
661 Geophysical Research Letters, 48, e2020GL090825, doi:https://doi.org/10.1029/2020GL090825, 2021.

662 Bador, M., Boé, J., Terray, L., Alexander, L. V., Baker, A., Bellucci, A., Haarsma, R., Koenigk, T., Moine, M.-P.,
663 Lohmann, K., Putrasahan, D. A., Roberts, C., Roberts, M., Scoccimarro, E., Schiemann, R., Seddon, J., Senan, R.,
664 Valcke, S., and Vanniere, B.: Im pact of Higher Spatial Atmospheric Resolution on Precipitation Extremes Over Land
665 in Global Climate Models, Journal of Geophysical Research: Atmospheres, 125, e2019JD032184,
666 doi:https://doi.org/10.1029/2019JD032184, 2020.

667 Bintanja, R., Katsman, C. A., and Selten, F. M.: Increased Arctic precipitation slows down sea ice melt and surface
668 warming, Oceanography, 31, 118–125, 2018.

669 Brodzik, M. J. and Stewart, J. S.: Near-Real-Time SSM/I-SSMIS EASE-Grid Daily Global Ice Concentration and Snow
670 Extent, Version 5, 2016.

671 Carmack, E., Polyakov, I., Padman, L., Fer, I., Hunke, E., Hutchings, J., Jackson, J., Kelley, D., Kwok, R., Layton, C.,
672 Melling, H., Perovich, D., Persson, O., Ruddick, B., Timmermans, M. L., Toole, J., Ross, T., Vavrus, S., and Winsor,
673 P.: Toward quantifying the increasing role of oceanic heat in sea ice loss in the new Arctic, Bulletin of the American
674 Meteorological Society, 96, 2079–2105, doi:10.1175/BAMS-D-13-00177.1, 2015.

675 Cavalieri, D. J., Gloersen, P., and Campbell, W. J.: Determination of sea ice parameters with the NIMBUS 7 SMMR,
676 Journal of Geophysical Research: Atmospheres, 89, 5355–5369, doi: https://doi.org/10.1029/JD089iD04p05355, 1984.

677 Cherchi, A., Fogli, P. G., Lovato, T., Peano, D., Iovino, D., Gualdi, S., Masina, S., Scoccimarro, E., Materia, S., Bellucci,
678 A., and Navarra, A.: Global Mean Climate and Main Patterns of Variability in the CMCC-CM2 Coupled Model,
679 Journal of Advances in Modeling Earth Systems, 11, 185–209, doi:10.1029/2018MS001369, 2019.

680 Comiso, J. C.: Characteristics of Arctic winter sea ice from satellite multispectral microwave observations, Journal of
681 Geophysical Research: Oceans, 91, 975–994, doi:https://doi.org/10.1029/JC091iC01p00975, 1986.

682 Davy, R. and Outten, S.: The Arctic Surface Climate in CMIP6: Status and Developments since CMIP5,
683 doi:10.1175/JCLI-D-19, URL https://doi.org/10.1175/JCLI-D-19-, 2020. Dee, D. P., Uppala, S. M., Simmons, A. J.,
684 Berrisford, P., Poli, P., Kobayashi, S., Andrae, U., Balmaseda, M. A., Balsamo, G., d P Bauer, et al.: The ERA-Interim
685 reanalysis: Configuration and performance of the data assimilation system, Quarterly Journal of the royal
686 meteorological society, 137, 553–597, 2011.

687 Deser, C., Lehner, F., Rodgers, K. B., Ault, T., Delworth, T. L., DiNezio, P. N., ... & Ting, M.: Insights from Earth system
688 model initial-condition large ensembles and future prospects. Nat. Clim. Change 10, 277–286, 2020.

689 Docquier, D. and Koenigk, T.: Observation-based selection of climate models projects Arctic ice-free summers around
690 2035, Communications Earth Environment, 2, 144, doi:10.1038/ s43247-021-00214-7, 2021.

691 Docquier, D., Grist, J. P., Roberts, M. J., Roberts, C. D., Semmler, T., Ponsoni, L., Mas sonnet, F., Sidorenko, D., Sein, D.
692 V., Iovino, D., Bellucci, A., and Fichefet, T.: Impact of model resolution on Arctic sea ice and North Atlantic Ocean

23

heat transport, Climate Dynamics, 53, 4989–5017, doi:10.1007/s00382-019-04840-y, 2019.

Docquier, D., Fuentes-Franco, R., Koenigk, T., and Fichefet, T.: Sea Ice-Ocean Interactions in the Barents Sea Modeled at Different Resolutions, Frontiers in Earth Science, 8, doi: 10.3389/feart.2020.00172, 2020.

Dumont, D., Kohout, A., and Bertino, L.: A wave-based model for the marginal ice zone including a floe breaking parameterization, J. Geophys. Res., 116, C04 001, 2011. Eyring, V., Bony, S., Meehl, G. A., Senior, C. A., Stevens, B., Stouffer, R. J., and Taylor, K. E.: Overview of the Coupled Model Intercomparison Project Phase 6 (CMIP6) experimental design and organization, Geoscientific Model Development, 9, 1937–1958, doi: 10.5194/gmd-9-1937-2016, 2016.

Fuentes-Franco, R. and Koenigk, T.: Sensitivity of the Arctic freshwater content and transport to model resolution, Climate Dynamics, 53, 1765–1781, doi:10.1007/s00382-019-04735-y, 2019.

Grist, J. P., Josey, S. A., New, A. L., Roberts, M., Koenigk, T., and Iovino, D.: Increasing Atlantic Ocean Heat Transport in the Latest Generation Coupled Ocean-Atmosphere Models: The Role of Air-Sea Interaction, Journal of Geophysical Research: Oceans, 123, 8624–8637, doi:https://doi.org/10.1029/2018JC014387, 2018.

Haarsma, R., Acosta, M., Bakhshi, R., Bretonnière, P. A., Caron, L. P., Castrillo, M., Corti, S., Davini, P., Exarchou, E., Fabiano, F., Fladrich, U., Franco, R. F., Garciá-Serrano, J., Hardenberg, J. V., Koenigk, T., Levine, X., Meccia, V. L., Noije, T. V., Oord, G. V. D., Palmeiro, F. M., Rodrigo, M., Ruprich-Robert, Y., Sager, P. L., Tourigny, E., Wang, S., Weele, M. V., and Wyser, K.: HighResMIP versions of EC-Earth: EC-Earth3P and EC-Earth3P-HR - Description, model computational performance and basic validation, Geoscientific Model Development, 13, 3507–3527, doi:10.5194/gmd-13-3507-2020, 2020.

Haarsma, R. J., Roberts, M. J., Vidale, P. L., Catherine, A., Bellucci, A., Bao, Q., Chang, P., Corti, S., Fučkar, N. S., Guemas, V., Hardenberg, J. V., Hazeleger, W., Kodama, C., Koenigk, T., Leung, L. R., Lu, J., Luo, J. J., Mao, J., Mizielinski, M. S., Mizuta, R., Nobre, P., Satoh, M., Scoccimarro, E., Semmler, T., Small, J., and Storch, J. S. V.: High Resolution Model Intercomparison Project (HighResMIP v1.0) for CMIP6, Geoscientific Model Development, 9, 4185–4208, doi:10.5194/gmd-9-4185-2016, 2016.

Horvat, C.: Marginal ice zone fraction benchmarks sea ice and climate model skill, Nature Communications, 12, 2221, doi:10.1038/s41467-021-22004-7, 2021.

Hunke, E.: Thickness sensitivities in the CICE sea ice model, Ocean Modelling - OCEAN MODEL, 34, 137–149, doi:10.1016/j.ocemod.2010.05.004, 2010.

Hunke, E., Allard, R., Blain, P., Blockley, E., Feltham, D., Fichefet, T., Garric, G., Grumbine, R., Lemieux, J.-F., Rasmussen, T., Ribergaard, M., Roberts, A., Schweiger, A., Tietsche, S., Tremblay, B., Vancoppenolle, M., and Zhang, J.: Should sea ice Modeling Tools Designed for Climate Research Be Used for Short-Term Forecasting?, Current Climate Change Reports, 6, 121–136, doi:10.1007/s40641-020-00162-y, 2020.

Ivanova, N., Pedersen, L. T., Tonboe, R. T., Kern, S., Heygster, G., Lavergne, T., Sørensen, A., Saldo, R., Dybkjær, G., Brucker, L., and Shokr, M.: Inter-comparison and evaluation of sea ice algorithms: towards further identification of

challenges and optimal approach using passive microwave observations, The Cryosphere, 9, 1797–1817, doi:10.5194/tc-9-1797-2015, 2015.

Jackson, L. C., Roberts, M. J., Hewitt, H. T., Iovino, D., Koenigk, T., Meccia, V. L., Roberts, C. D., Ruprich-Robert, Y., and Wood, R. A.: Impact of ocean resolution and mean state on the rate of AMOC weakening, Climate Dynamics, 55, 1711–1732, doi: 10.1007/s00382-020-05345-9, 2020.

Jungclaus, J. H., Fischer, N., Haak, H., Lohmann, K., Marotzke, J., Matei, D., Mikolajewicz, U., Notz, D., and Storch, J. S. V.: Characteristics of the ocean simulations in the Max Planck Institute Ocean Model (MPIOM) the ocean component of the MPI-Earth system model, Journal of Advances in Modeling Earth Systems, 5, 422–446, doi:10.1002/jame.20023, 2013.

Kalnay, E., Kanamitsu, M., Kistler, R., Collins, W., Deaven, D., Gandin, L., Iredell, M., Saha, S., White, G., Woollen, J., Zhu, Y., Chelliah, M., Ebisuzaki, W., Higgins, W., Janowiak, J., Mo, K. C., Ropelewski, C., Wang, J., Leetmaa, A., Reynolds, R., Jenne, R., and Joseph, D.: The NCEP/NCAR 40-Year Reanalysis Project, Bulletin of the American Meteorological Society, 77, 437 – 472, doi:10.1175/1520-0477(1996)077<0437:TNYRP>2.0.CO;2, 1996.

Kay, J. E.,. Holland, M. M, and Jahn, A.: Inter-annual to multi-decadal Arctic sea ice extent trends in a warming world, Geophys. Res. Lett., 38, L15708, doi:10.1029/2011GL048008, 2011.

Keen, A., Blockley, E., Bailey, D. A., Debernard, J. B., Bushuk, M., Delhaye, S., Docquier, D., Feltham, D., Massonnet, F., O'Farrell, S., Ponsoni, L., Rodriguez, J. M., Schroeder, D., Swart, N., Toyoda, T., Tsujino, H., Vancoppenolle, M., and Wyser, K.: An inter-comparison of the mass budget of the Arctic sea ice in CMIP6 models, The Cryosphere, 15, 951–982, doi:10. 5194/tc-15-951-2021, 2021.

Koenigk, T., Fuentes-Franco, R., Meccia, V. L., Gutjahr, O., Jackson, L. C., New, A. L., Ortega, P., Roberts, C. D., Roberts, M. J., Arsouze, T., Iovino, D., Moine, M. P., and Sein, D. V.: Deep mixed ocean volume in the Labrador Sea in HighResMIP models, Climate Dynamics, 57, 1895–1918, doi:10.1007/s00382-021-05785-x, 2021.

Kwok, R. and Untersteiner, N.: The thinning of Arctic sea ice, Physics Today, 64, 36–41, doi: 10.1063/1.3580491, 2011.

Labe, Z., Magnusdottir, G., and Stern, H.: Variability of Arctic Sea Ice Thickness Us ing PIOMAS and the CESM Large Ensemble, Journal of Climate, 31, 3233 – 3247, doi: 10.1175/JCLI-D-17-0436.1, 2018.

Lavergne, T., Sørensen, A. M., Kern, S., Tonboe, R., Notz, D., Aaboe, S., Bell, L., Dybkjær, G., Eastwood, S., Gabarro, C., Heygster, G., Killie, M. A., Kreiner, M. B., Lavelle, J., Saldo, R., Sandven, S., and Pedersen, L. T.: Version 2 of the EUMETSAT OSI SAF and ESA CCI sea ice concentration climate data records, The Cryosphere, 13, 49–78, doi:10.5194/tc-13-49-2019, 2019.

Li, D., Zhang, R., and Knutson, T. R.: On the discrepancy between observed and CMIP5 multi-model simulated Barents Sea winter sea ice decline, Nature Communications, 8, 14 991, doi:10.1038/ncomms14991, 2017.

Lohmann, K., Putrasahan, D. A., von Storch, J.-S., Gutjahr, O., Jungclaus, J. H., and Haak, H.: Response of Northern North Atlantic and Atlantic Meridional Overturning Circulation to Reduced and Enhanced Wind Stress Forcing, Journal of Geophysical Research: Oceans, 126, e2021JC017 902, doi:https://doi.org/10.1029/2021JC017902, 2021.

Madec, G., Bourdallé-Badie, R., Chanut, J., Clementi, E., Coward, A., Ethé, C., Iovino, D., Lea, D., Lévy, C., Lovato, T., Martin, N., Masson, S., Mocavero, S., Rousset, C., Storkey, D., Müeller, S., Nurser, G., Bell, M., Samson, G., Mathiot, P., Mele, F., and Moulin, A.: NEMO ocean engine, doi:10.5281/ZENODO.6334656, 2016.

Maher, N., Lehner, F., and Marotzke, J.: Quantifying the role of internal variability in the temperature we expect to observe in the coming decades. Environ. Res. Lett. 15, 054014, 2020.

Massonnet, F., Vancoppenolle, M., Goosse, H., Docquier, D., Fichefet, T., and Blanchard Wrigglesworth, E.: Arctic sea ice change tied to its mean state through thermodynamic processes, Nature Climate Change, 8, 599–603, doi:10.1038/s41558-018-0204-z, 2018.

Meccia, V. L., Iovino, D., and Bellucci, A.: North Atlantic gyre circulation in PRIMAVERA models, Climate Dynamics, 56, 4075–4090, doi:10.1007/s00382-021-05686-z, 2021.

Meier, WN, Stroeve, J and Fetterer, F. Whither Arctic sea ice? A clear signal of decline regionally, seasonally and extending beyond the satellite record. Ann. Glaciol., 46, 428–434.doi: 10.3189/172756407782871170, 2007

Meier, W. N., Peng, G., Scott, D. J., and Savoie, M. H. Verification of a New NOAA/NSIDC Passive Microwave sea ice Concentration Climate Record. Polar Res. 33 (1), 21004. doi:10.3402/polar.v33.21004, 2014.

Meier, W. N., Fetterer, F., Windnagel, A. K., and Stewart, J. S.: NOAA/NSIDC Climate Data Record of Passive Microwave Sea Ice Concentration, Version 4, doi:10.7265/efmz-2t65, 2021.

Muilwijk, M., Ilicak, M., Cornish, S. B., Danilov, S., Gelderloos, R., Gerdes, R., Haid, V., Haine, T. W. N., Johnson, H. L., Kostov, Y., Kovács, T., Lique, C., Marson, J. M., Myers, P. G., Scott, J., Smedsrud, L. H., Talandier, C., and Wang, Q.: Arctic Ocean Response to Greenland Sea Wind Anomalies in a Suite of Model Simulations, Journal of Geophysical Research: Oceans, 124, 6286–6322, doi:https://doi.org/10.1029/2019JC015101, 2019.

Müller, W. A., Jungclaus, J. H., Mauritsen, T., Baehr, J., Bittner, M., Budich, R., Bunzel, F., Esch, M., Ghosh, R., Haak, H., Ilyina, T., Kleine, T., Kornblueh, L., Li, H., Modali, K., Notz, D., Pohlmann, H., Roeckner, E., Stemmler, I., Tian, F., and Marotzke, J.: A Higher-resolution Version of the Max Planck Institute Earth System Model (MPI-ESM1.2-HR), Journal of Advances in Modeling Earth Systems, 10, 1383–1413, doi:10.1029/2017MS001217, 2018.

Notz, D. and Community, S.: Arctic Sea Ice in CMIP6, Geophysical Research Letters, 47, e2019GL086749, doi:https://doi.org/10.1029/2019GL086749, 2020.

Notz, D. and Stroeve, J.: Observed Arctic sea ice loss directly follows anthropogenic CO2 emission, Science, 354, 747–750, doi:10.1126/science.aag2345, 2016.

Onarheim, I. H., Eldevik, T., Smedsrud, L. H., and Stroeve, J. C.: Seasonal and Regional Manifestation of Arctic Sea Ice Loss, Journal of Climate, 31, 4917 – 4932, doi: 10.1175/JCLI-D-17-0427.1, 2018.

Ono, J., Komuro, Y., and Tatebe, H.: Impact of sea ice thickness initialized in April on Arctic sea ice extent predictability with the MIROC climate model, Annals of Glaciology, 61, 97–105, doi:10.1017/aog.2020.13, 2020.

Papalexiou, S. M., Rajulapati, C. R., Clark, M. P., and Lehner, F.: Robustness of CMIP6 Historical Global Mean Temperature Simulations: Trends, Long-Term Persistence, Auto correlation, and Distributional Shape, Earth's Future,

795   8, e2020EF001 667, doi:https://doi.org/10.1029/2020EF001667, 2020.

796 Park, H., Watanabe, E., Kim, Y., Polyakov, I., Oshima, K., Zhang, X., Kimball, J. S., and Yang, D.: Increasing riverine
797   heat influx triggers Arctic sea ice decline and oceanic and atmospheric warming, Science Advances, 6, eabc4699,
798   doi:10.1126/sciadv.abc4699, URL https://www. science.org/doi/abs/10.1126/sciadv.abc4699, 2020.

799 Parkinson, C. L., Cavalieri, D. J., Gloersen, P., Zwally, H. J. and Comiso, J. C.: Arctic sea ice extents, areas, and trends,
800 1978–1996. J. Geophys. Res., 104(C9), 20,837–20,856, 1999.

801 Paul, F., Mielke, T., Schwarz, C., Schröder, J., Rampai, T., Skatulla, S., Audh, R. R., Hepworth, E., Vichi, M., and
802   Lupascu, D. C.: Frazil Ice in the Antarctic Marginal Ice Zone, Journal of Marine Science and Engineering, 9,
803   doi:10.3390/jmse9060647, URL https://www.mdpi.com/2077-1312/9/6/647, 2021.

804 Peng, G., and Meier, W.: Temporal and regional variability of Arctic sea ice coverage from satellite data, Annals of
805   Glaciology, 59, 76pt2, 191-200. doi:10.1017/aog.2017.32, 2018.

806 Perovich, D., Meier, W., Tschudi, M., Hendricks, S., Petty, A. A., Divine, D., Farrell, S., Gerland, S., Haas, C., Kaleschke,
807   L., Pavlova, O., Ricker, R., Tian-Kunze, X., Webster, M., and Wood, K.: NOAA Arctic Report Card 2020,
808   doi:10.25923/n170-9h57, 2020.

809 Roberts, C. D., Senan, R., Molteni, F., Boussetta, S., Mayer, M., and Keeley, S. P.: Climate model configurations of the
810   ECMWF integrated forecasting system (ECMWF-IFS cycle43r1) for HighResMIP, Geoscientific Model Development,
811   11, 3681–3712, doi:10.5194/ gmd-11-3681-2018, 2018.

812 Roberts, M. J., Jackson, L. C., Roberts, C. D., Meccia, V., Docquier, D., Koenigk, T., Ortega, P., Moreno-Chamarro, E.,
813   Bellucci, A., Coward, A., Drijfhout, S., Exarchou, E., Gutjahr, O., Hewitt, H., Iovino, D., Lohmann, K., Putrasahan,
814   D., Schiemann, R., Seddon, J., Terray, L., Xu, X., Zhang, Q., Chang, P., Yeager, S. G., Castruccio, F. S., Zhang, S., and
815   Wu, L.: Sensitivity of the Atlantic Meridional Overturning Circulation to Model Resolution in CMIP6 HighResMIP
816   Simulations and Implications for Future Changes, Journal of Advances in Modeling Earth Systems, 12,
817   doi:10.1029/2019MS002014, 2020.

818 Rolph, R. J., Feltham, D. L., and Schröder, D.: Changes of the Arctic marginal ice zone during the satellite era, The
819   Cryosphere, 14, 1971–1984, doi:10.5194/tc-14-1971-2020, 2020.

820 Senftleben, D., A. Lauer, and A. Karpechko: Constraining Uncertainties in CMIP5 Projections of September Arctic Sea Ice
821 Extent with Observations. J. Climate, 33, 1487–1503, https://doi.org/10.1175/JCLI-D-19-0075.1, 2020.

822 Serreze, M. C. and Meier, W. N.: The Arctic's sea ice cover: trends, variability, predictability, and comparisons to the
823   Antarctic, Annals of the New York Academy of Sciences, 1436, 36–53, doi:10.1111/nyas.13856, 2019.

824 Shu, Q., Wang, Q., Song, Z., Qiao, F., Zhao, J., Chu, M., and Li, X.: Assessment of Sea Ice Extent in CMIP6 With
825   Comparison to Observations and CMIP5, Geophysical Research Letters, 47, e2020GL087965,
826   doi:https://doi.org/10.1029/2020GL087965, 2020.

827 Smedsrud, L. H., Ingvaldsen, R., Nilsen, J. E. Ø., and Skagseth, Ø.: Heat in the Barents Sea: transport, storage, and
828   surface fluxes, Ocean Science, 6, 219–234, doi:10.5194/os-6-219-2010, 2010.

Smith, M. M., von Albedyll, L., Raphael, I. A., Lange, B. A., Matero, I., Salganik, E., Web ster, M. A., Granskog, M. A., Fong, A., Lei, R., and Light, B.: Quantifying false bottoms and under-ice meltwater layers beneath Arctic summer sea ice with fine-scale observations, Elementa: Science of the Anthropocene, 10, 000116, doi:10.1525/elementa.2021.000116, 2022.

Strandberg, G. and Lind, P.: The importance of horizontal model resolution on simulated precipitation in Europe – from global to regional models, Weather and Climate Dynamics, 2, 181–204, doi:10.5194/wcd-2-181-2021, 2021.

Stroeve, J., Barrett, A., Serreze, M., and Schweiger, A.: Using records from submarine, aircraft and satellites to evaluate climate model simulations of Arctic sea ice thickness, The Cryosphere, 8, 1839–1854, doi:10.5194/tc-8-1839-2014, 2014.

Strong, C., Foster, D., Cherkaev, E., Eisenman, I., and Golden, K. M.: On the Definition of Marginal Ice Zone Width, J. Atmos. Ocean. Tech., 34, 1565–1584, https://doi.org/10.1175/JTECH-D-16-0171.1, 2017.

Swart, N. C., Fyfe, J. C., Hawkins, E., Kay, J. E., and Jahn, A.: Influence of internal variability on Arctic sea-ice trends. Nature Climate Change, 5, 86-89. doi:10.1038/nclimate2483, 2015.

Tápias, G., Lizotte, M., Kieber, M., D. Randelhoff, A., Xue, R., Dinasquet, L., Babin, J., Rehm, M., and Levasseur, E.: DMS emissions from the Arctic marginal ice zone, Elementa: Science of the Anthropocene, 9, doi:10.1525/elementa.2020.00113, 2021.

Voldoire, A., Saint-Martin, D., Sénési, S., Decharme, B., Alias, A., Chevallier, M., Colin, J., Guérémy, J. F., Michou, M., Moine, M. P., Nabat, P., Roehrig, R., y Mélia, D. S., Séférian, R., Valcke, S., Beau, I., Belamari, S., Berthet, S., Cassou, C., Cattiaux, J., Deshayes, J., Douville, H., Ethé, C., Franchistéguy, L., Geoffroy, O., Lévy, C., Madec, G., Meurdesoif, Y., Msadek, R., Ribes, A., Sanchez-Gomez, E., Terray, L., and Waldman, R.: Evaluation of CMIP6 DECK Experiments With CNRM-CM6-1, Journal of Advances in Modeling Earth Systems, 11, 2177–2213, doi:10.1029/2019MS001683, 2019.

Wadhams, P. and Deacon, G. E. R.: Sea-ice topography of the Arctic Ocean in the region 70∘ W to 25∘ E, Philosophical Transactions of the Royal Society of London. Series A, Mathematical and Physical Sciences, 302, 45–85, doi:10.1098/rsta.1981.0157, 1981.

Wang, M., and Overland, J. E.: A sea ice free summer Arctic within 30 years: An update from CMIP5 models, Geophys. Res. Lett., 39, L18501, doi:10.1029/2012GL052868, 2020.

Wang, X., Key, J., Kwok, R., and Zhang, J.: Comparison of Arctic sea ice thickness from satellites, aircraft, and PIOMAS data, Remote Sensing, 8, doi:10.3390/RS8090713, 2016. Watts, M., Maslowski, W., Lee, Y. J., Kinney, J. C., and Osinski, R.: A Spatial Evaluation of Arctic Sea Ice and Regional Limitations in CMIP6 Historical Simulations, Journal of Climate, 34, 6399–6420, doi:10.1175/JCLI-D-20-0491.1, 2021.

Williams, K. D., Copsey, D., Blockley, E. W., Bodas-Salcedo, A., Calvert, D., Comer, R., Davis, P., Graham, T., Hewitt, H. T., Hill, R., Hyder, P., Ineson, S., Johns, T. C., Keen, A. B., Lee, R. W., Megann, A., Milton, S. F., Rae, J. G. L., Roberts, M. J., Scaife, A. A., Schiemann, R., Storkey, D., Thorpe, L., Watterson, I. G., Walters, D. N., West, A., Wood,

28

863 R. A., Woollings, T., and Xavier, P. K.: The Met Office Global Coupled Model 3.0 and 3.1 (GC3.0 and GC3.1)

864 Configurations, Journal of Advances in Modeling Earth Systems, 10, 357–380,

865 doi:https://doi.org/10.1002/2017MS001115, 2018.

866 Zhang, J. and Rothrock, D. A.: Modeling Global Sea Ice with a Thickness and Enthalpy Distribution Model in

867 Generalized Curvilinear Coordinates, 2003.

868 Zhang, X.: Sensitivity of Arctic Summer Sea Ice Coverage to Global Warming Forcing: Toward Reducing Uncertainty in

869 Arctic Climate Change Projections, Tellus A, 62, 220 – 227, doi: 10.1111/j.1600-0870.2010.00441.x, 2010.

870

871 **Figures**

872
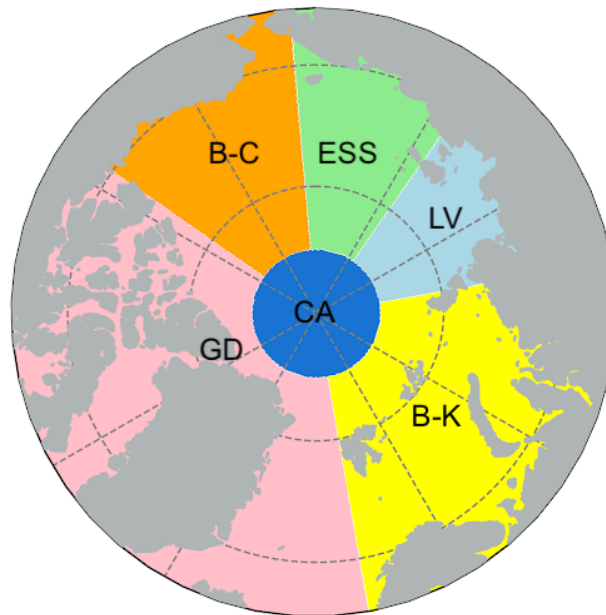
873

874

875 **Figure 1: Map of sub-regions used in the regional analysis: Central Arctic Basin (CA), Barents and Kara Seas (B-K), Laptev Sea**
876 **(LV), East Siberian Sea (ESS), Beaufort and Chukchi Seas (B-C), Canadian Arctic Archipelago and Greenland coast (GD).**

877

878

879

880

881

29

a)

886 b)
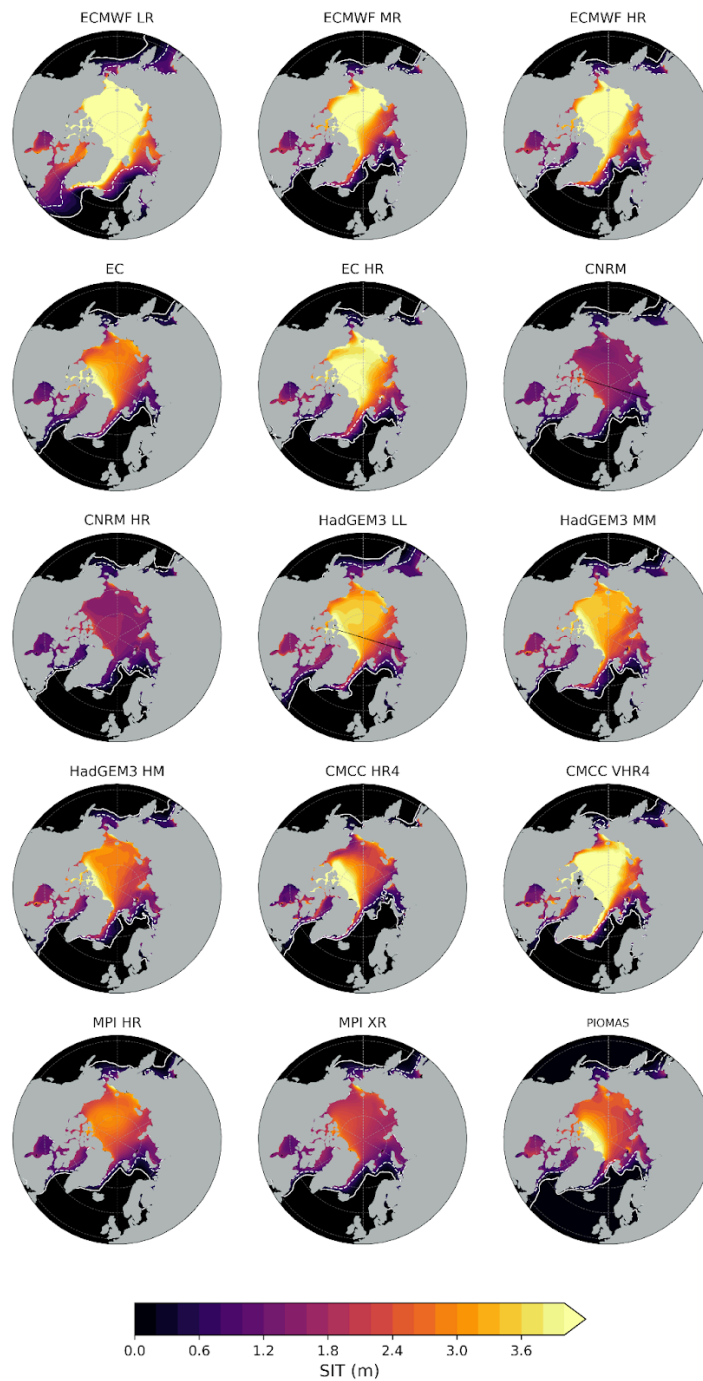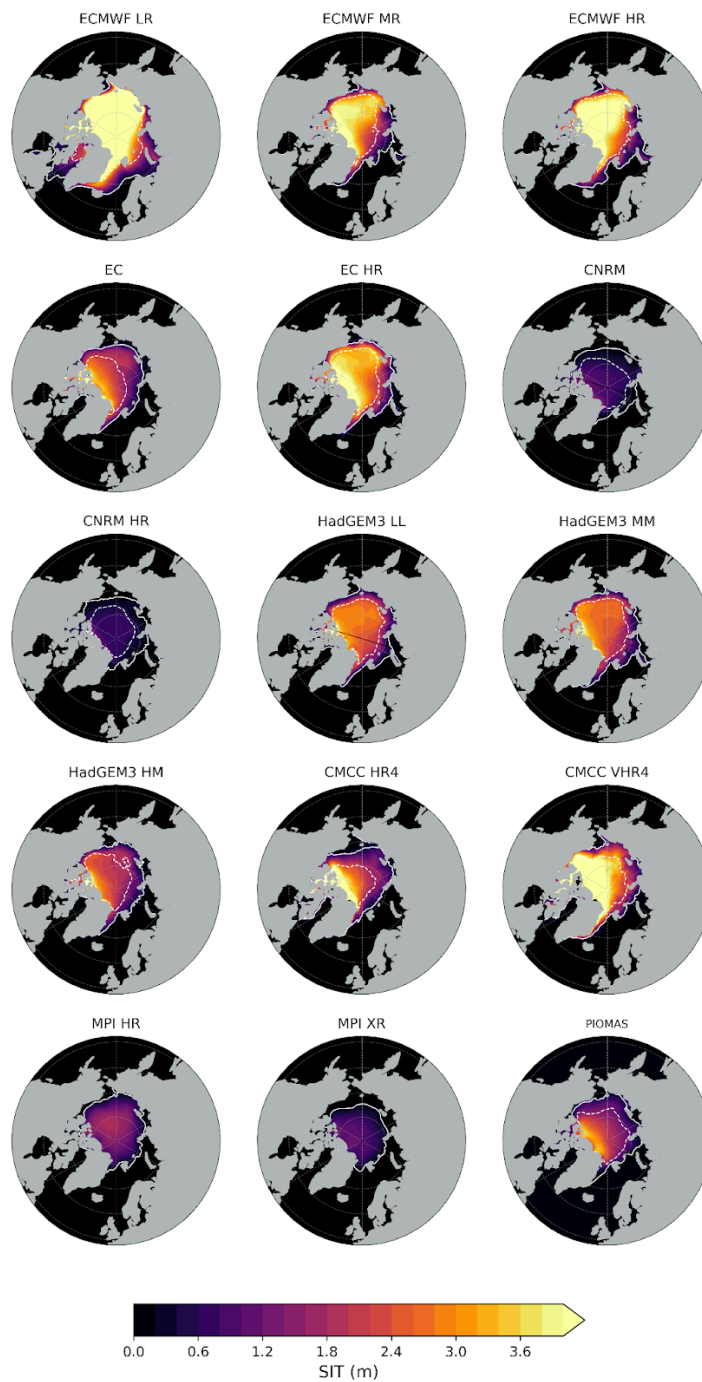
Figure 2: The 1979-2014 climatological mean sea ice thickness from the model outputs and PIOMAS in March (a) and September (b). White contours show the edges of 15% (solid) and 80% (dashed) sea ice concentration from each model. SIC from CDR is used for PIOMAS.

31
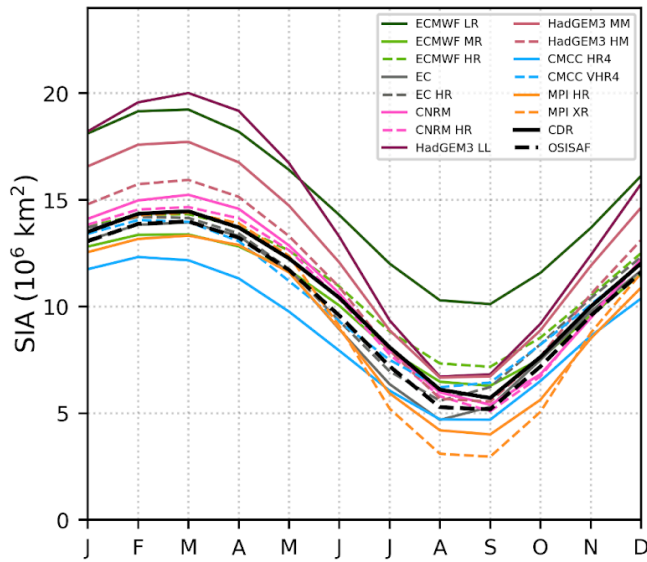
891 **(a)**   **(b)**
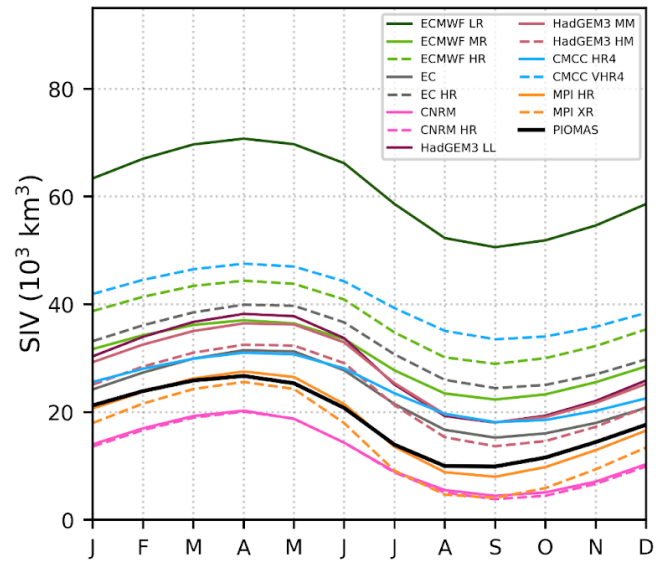
892

893 **Figure 3: The 1979-2014 seasonal cycle in SIA (a) and SIV (b) from HighResMIP hist-1950 model outputs against CDR and**
894 **OSISAF for SIA and PIOMAS for SIV.**

895
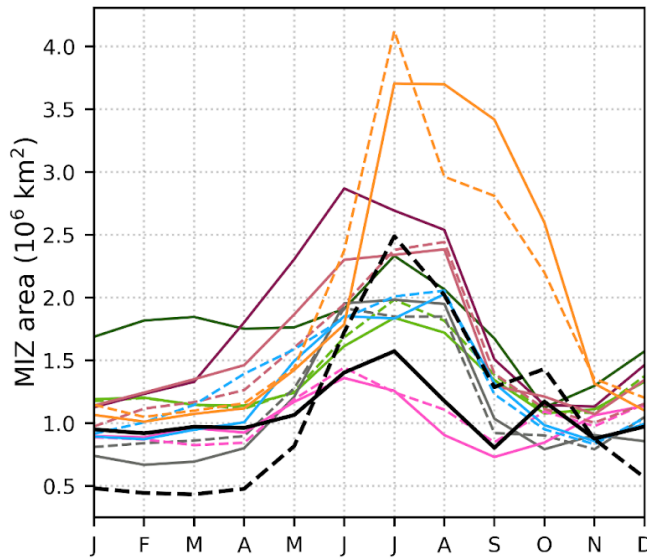
896 **(a)**   **(b)**
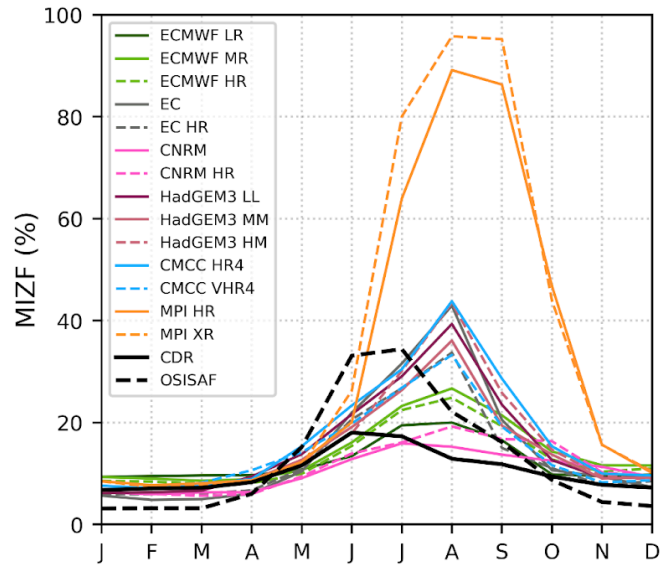
897

898 **Figure 4: The 1979-2014 seasonal cycle in the MIZ area (a) and MIZF (b) from HighResMIP hist-1950 model outputs and**
899 **satellite products.**

900

(a)

b)
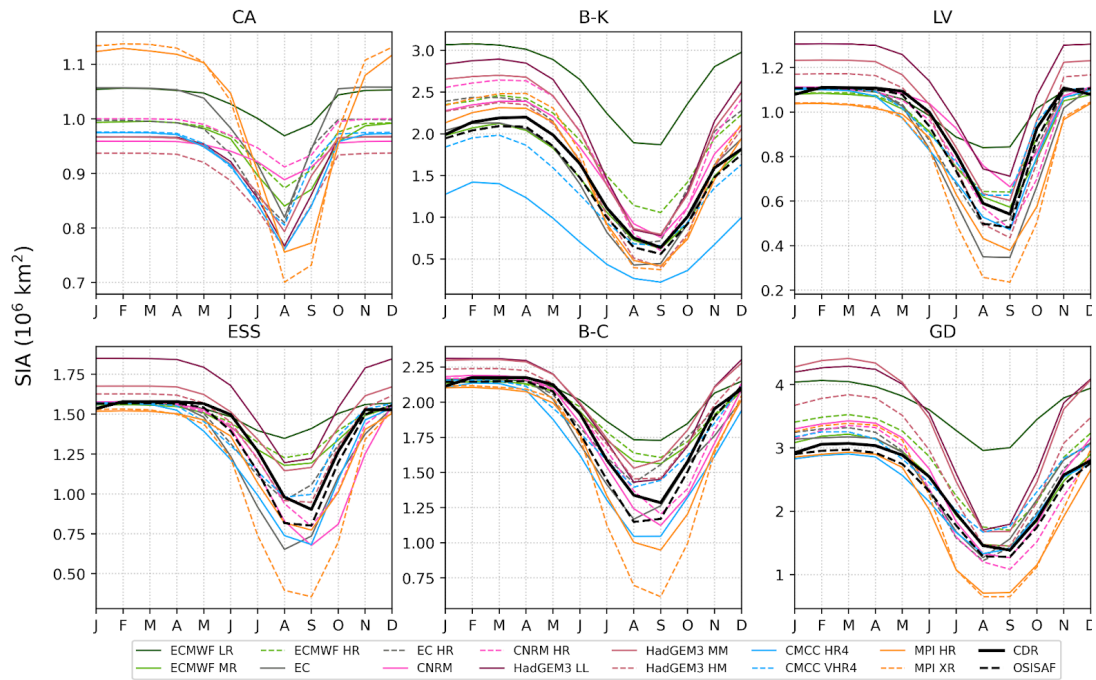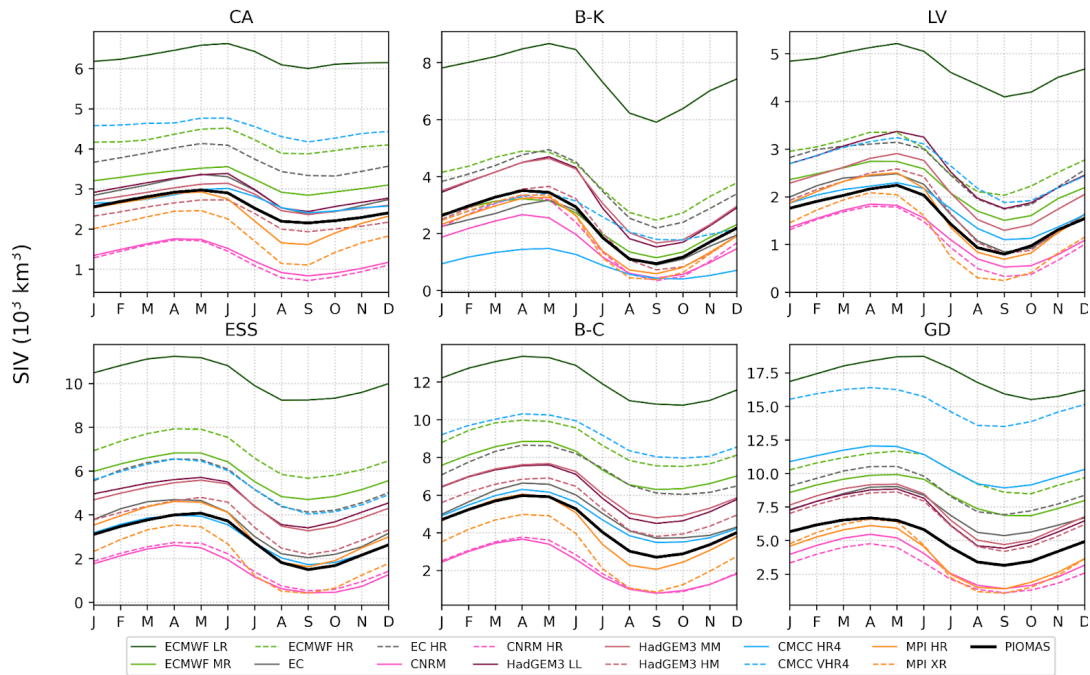
Figure 5: The 1979-2014 seasonal cycle in a) SIA and b) SIV in the Arctic sub-regions from HighResMIP hist-1950 model outputs against CDR and OSISAF for SIA and PIOMAS for SIV.

33

(a)

912
913
914
915
916
917
918
919
920

b)

921
922
923
924
925
926
927
928
929
930
931
932

Figure 6: Monthly anomalies of SIA (a) and SIV (b) over 1979-2014 from HighResMIP model outputs and reference products.
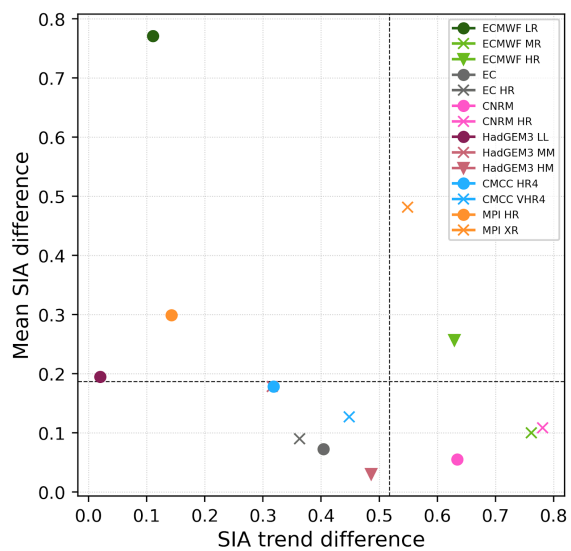
933
934
935
936
937
938
939
940
941
942
943
944
945
946
947
948
949
950
951
952
953
954

(a)

b)
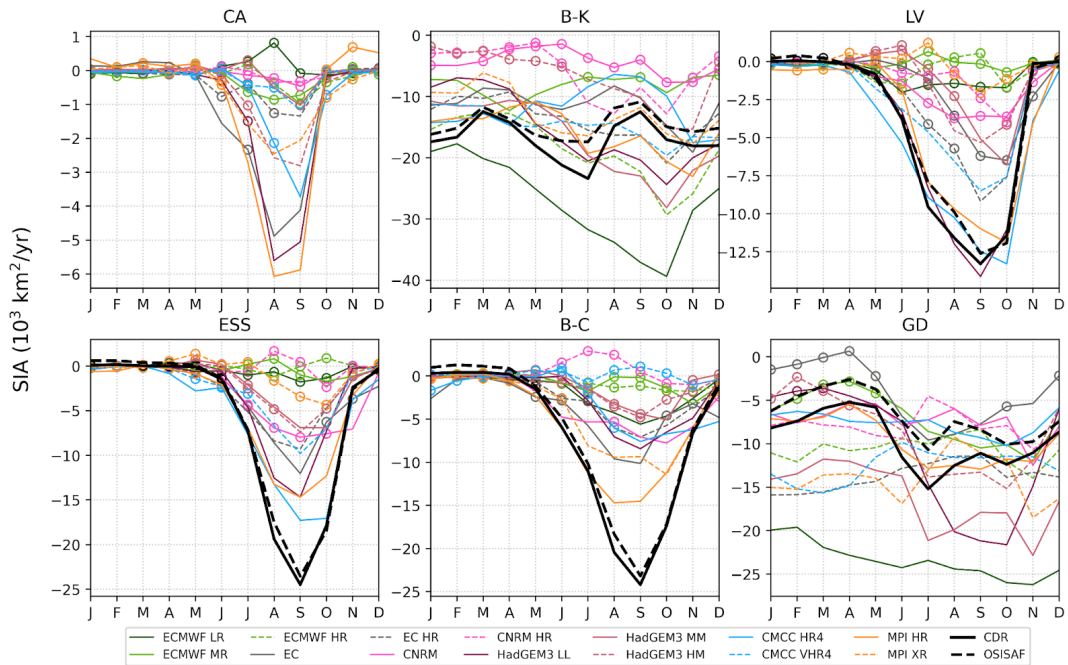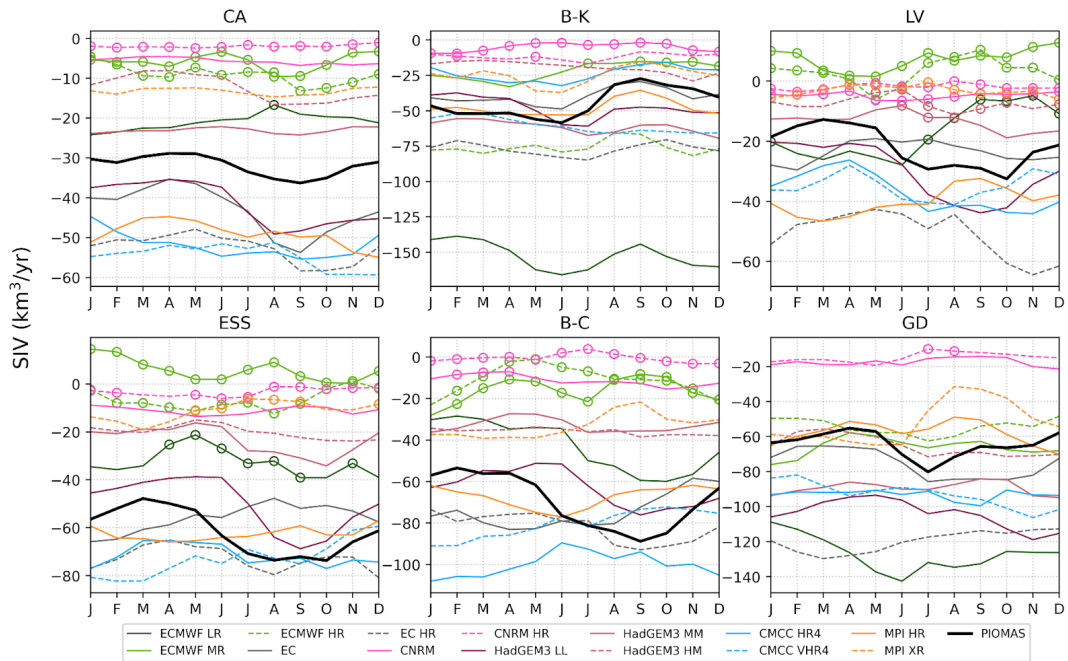
Figure 7: The 1979-2014 monthly trends in SIA (a) and SIV (b) in the Arctic sub-regions for HighResMIP hist-1950 model outputs against CDR and OSISAF for SIA and PIOMAS for SIV. Dots indicate non-significant trends.
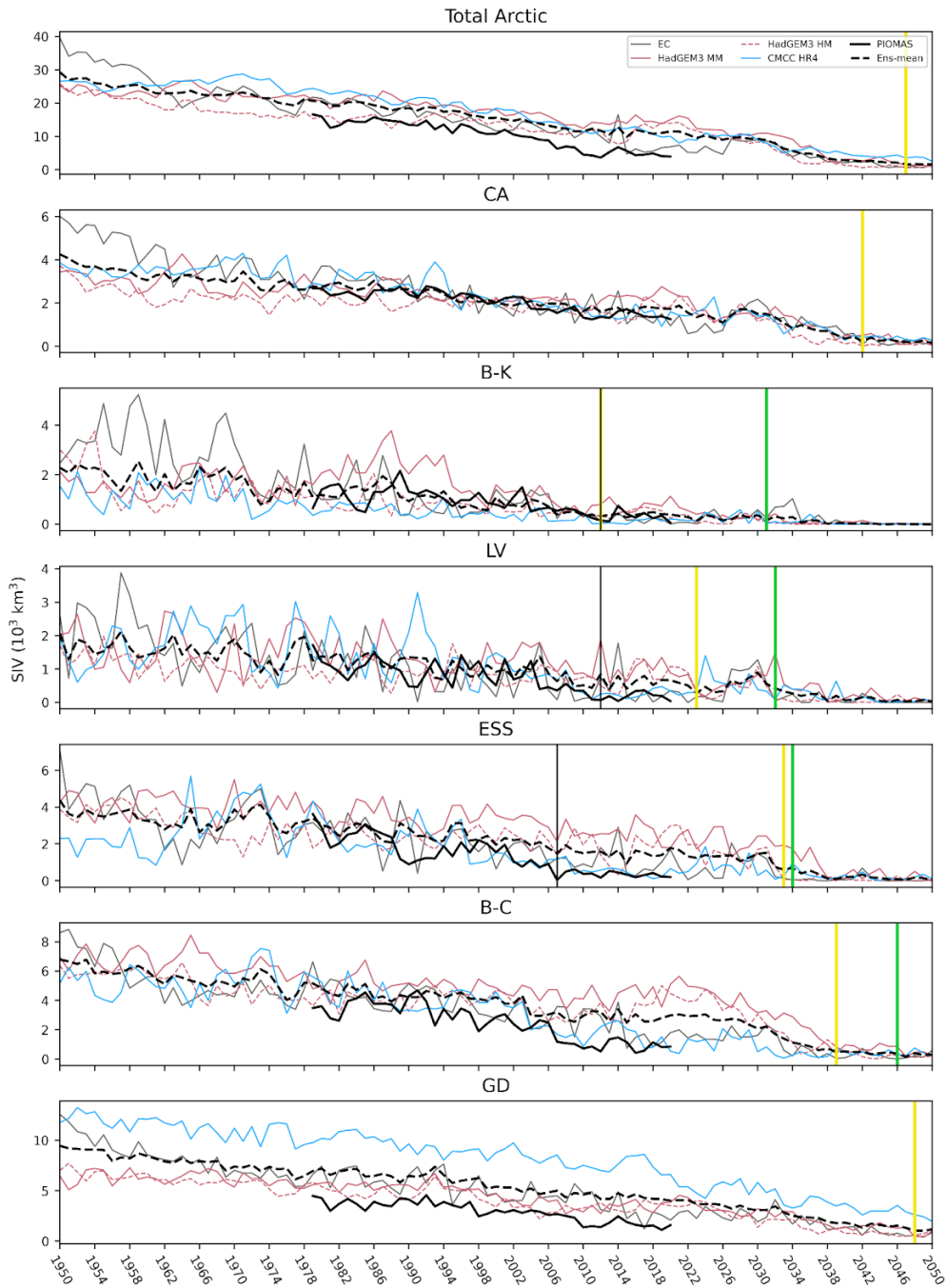
35

(a)

Figure 8. Normalized difference in mean September SIA against September SIA trend over 1979-2014 (a). Same for SIV (b). The difference is computed with reference to CDR (for SIA) and PIOMAS (for SIV). Dashed lines indicate 75th percentile for a set of the model outputs excluding ECMWF-IFS.
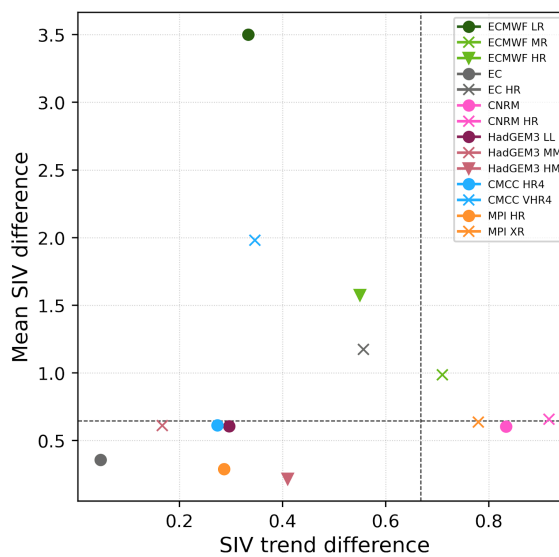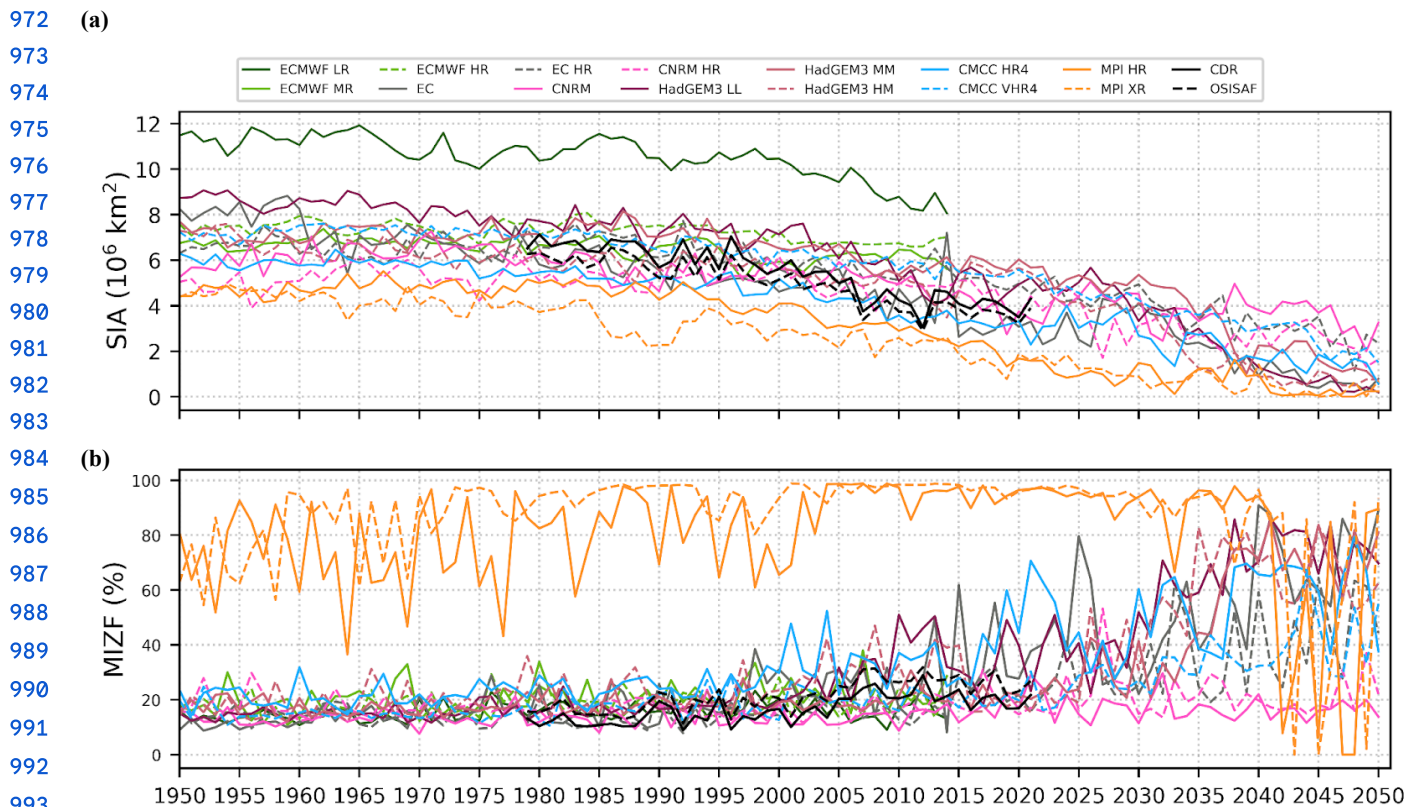
Figure 9: Time series of September SIV from 1950 to 2050 using HighResMIP historical and future runs and PIOMAS for the entire Arctic and sub-regions. The multi-model mean SIV with model selection is shown by dashed line. The vertical lines indicate the time of ice-free conditions: green colour for the multi-model mean without model selection, yellow for the multi-model mean with model selection, and black for CDR. Free-ice conditions signify that SIA falls below 10^6 km² for the total Arctic and reaches 25% of the CDR SIA averaged over 1980-2010 for the sub-regions.
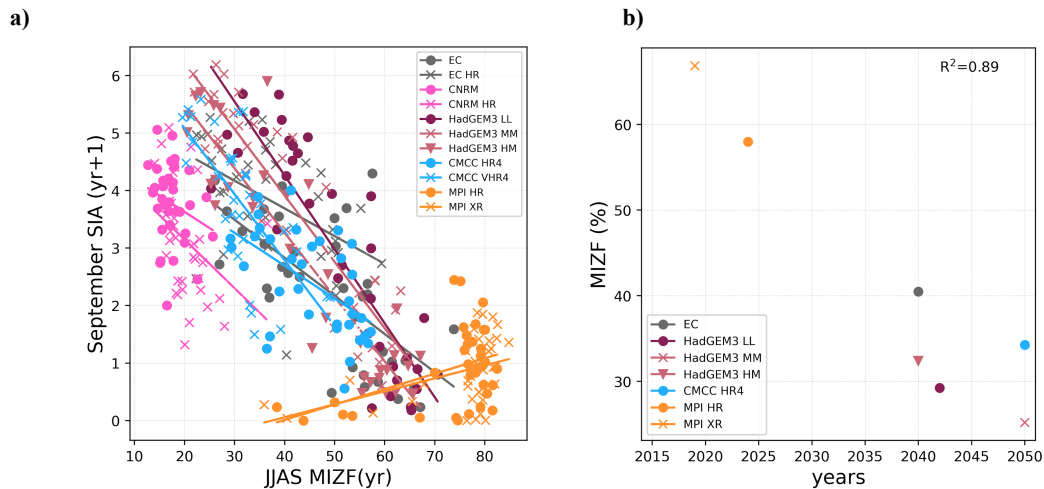
(a)

(b)

Figure 10: Time series of September SIA (a) and MIZF (b) from 1950 to 2050 using HighResMIP historical and future runs and satellite products (CDR and OSISAF).

a)

b)

Figure 11: June, July, August, and September (JJAS) MIZF mean against September SIA with one year lag over 2015-2050 (a); Timing of first ice-free Arctic against JJAS MIZF in 2015 (b).